

UNIVERZA V LJUBLJANI  
FAKULTETA ZA FARMACIJO

MATEJ HOLC

**IZRAŽANJE IZBRANIH GENOV  
V MAKROFAGOM PODOBNIH CELICAH, OKUŽENIH S  
THEILERJEVIM VIRUSOM MIŠJEGA ENCEFALOMIELITISA**

**THE EXPRESSION OF SPECIFIC GENES IN  
THEILER'S MURINE ENCEPHALOMYELITIS VIRUS-INFECTED  
MACROPHAGE-LIKE CELLS**

Ljubljana, 2013

This Master's thesis was performed at the Department of Pharmaceutical Biotechnology and Molecular Biology (MICH), Faculteit Geneeskunde & Farmacie, Vrije Universiteit Brussel, Brussels, Belgium, and at the Faculty of Pharmacy, University of Ljubljana, Ljubljana, Slovenia. The Master's thesis was created under the mentorship of Prof. Dr. Borut Štrukelj, and the co-mentorship of Prof. Dr. Ann Massie.

## **ACKNOWLEDGEMENTS**

I would like to thank Prof. Dr. Ann Massie and the entire department of MICH for the opportunity to conduct the research for this thesis at their facilities. I am thankful to the whole team at the department for their continuous support and assistance during my time in Belgium. Most of all, I would like to thank Ellen Merckx, who guided me through my research process, and helped me immensely in the efforts to create this Master's thesis.

Special thanks to Dr. Peter Kronenberger at Erasmushogeschool Brussel, without whose academic drive, technical skills and helpfulness, this research would not have been possible.

I would like to thank Prof. Dr. Borut Štrukelj at the Faculty of Pharmacy, University of Ljubljana, for the professional guidance and kind advice throughout the process of creating this Master's thesis.

My thanks also go to Assist. Prof. Dr. Lucija Peterlin Mašič and Doc. Dr. Simon Žakelj for their review and commentary on the contents of the thesis.

Many thanks to everybody who was, and still is, there for me: my family, my friends, and my girlfriend.

## **STATEMENT**

I hereby state that I have performed and written this Master's thesis solely by myself under the mentorship of Prof. Dr. Borut Štrukelj, and the co-mentorship of Prof. Dr. Ann Massie.

Matej Holc

Ljubljana, March 2013

# TABLE OF CONTENTS

<b>TABLE OF CONTENTS</b> .....	3
<b>ABSTRACT</b> .....	5
<b>POVZETEK</b> .....	6
<b>LIST OF ABBREVIATIONS</b> .....	7
<b>1. INTRODUCTION</b> .....	9
1.1. Theiler's Murine Encephalomyelitis Virus.....	9
1.1.1. Properties.....	9
1.1.2. Pathogenicity.....	10
1.1.3. GDVII group and GDVII strain .....	10
1.1.4. Theiler's Original group and DA strain .....	11
1.1.5. Viral persistence.....	12
1.2. Theiler's Murine Encephalomyelitis Virus in multiple sclerosis research .....	13
1.2.1. Multiple sclerosis .....	13
1.2.2. Experimental models of multiple sclerosis .....	15
1.2.3. TMEV persistent infection <i>in vivo</i> as a model of multiple sclerosis.....	16
1.2.4. TMEV persistent infection <i>in vitro</i> .....	18
1.2.5. RAW264.7 macrophage-like cells .....	19
1.2.6. DRAW cells .....	20
<b>2. AIMS AND HYPOTHESIS</b> .....	21
2.1. Aims of the thesis.....	21
2.2. Working hypothesis.....	22
<b>3. MATERIALS AND METHODS</b> .....	23
3.1. Cell cultivation.....	23
3.1.1. Materials.....	23
3.1.2. Methods.....	24
3.2. Sampling .....	24
3.2.1. Materials.....	24
3.2.2. Cell harvesting.....	25
3.2.3. Starting a sampling experiment.....	25
3.2.4. Sampling .....	26
3.3. Sample characterization .....	27
3.3.1. Cell viability assay .....	27
3.4. Total RNA extraction with DNase digestion .....	28

3.4.1. Materials.....	28
3.4.2. Protocol .....	28
3.5. Reverse transcription real-time quantitative polymerase chain reaction.....	30
3.5.1. Method background.....	30
3.5.2. Materials.....	32
3.5.3. Equipment .....	34
3.5.4. Primer design.....	34
3.5.5. Reverse transcription.....	36
3.5.6. Real-time quantitative polymerase chain reaction .....	37
3.5.7. Optimization.....	38
3.5.8. Control reactions .....	39
3.6. Data analysis .....	40
3.6.1. Amplification efficiency.....	40
3.6.2. Relative quantification .....	41
3.6.3. Statistical data analysis.....	42
3.6.4. Melting curve analysis .....	43
<b>4. RESULTS.....</b>	<b>44</b>
4.1. Cell viability.....	44
4.2. RNA extraction .....	45
4.3. Relative quantification of gene expression .....	46
4.3.1. Amplification efficiency.....	46
4.3.2. Relative quantification .....	48
4.3.3. Melting curve analysis .....	52
<b>5. DISCUSSION .....</b>	<b>53</b>
5.1. Target gene expression.....	53
5.1.1. Dusp6 .....	53
5.1.2. Gng12.....	54
5.1.3. The ubiquitin pathway: Ubqln2 and Tifa .....	55
5.1.4. Gja1 .....	58
5.1.5. Apoptosis: Prkar2b and Bcl2.....	59
5.1.6. Ccl5 .....	61
5.1.7. Adrb2.....	62
5.1.8. Slc7a11 .....	64
5.2. Conclusion.....	65
<b>REFERENCES.....</b>	<b>68</b>

## ABSTRACT

Theiler's Murine Encephalomyelitis Virus (TMEV) is an enteric pathogen of mice that can also cause infection of the central nervous system (CNS). Two groups of TMEV strains exist. The neurovirulent GDVII group includes the GDVII strain and induces an acute encephalomyelitis after intracerebral inoculation, which is mostly fatal. The persistent Theiler's Original (TO) group includes the DA strain, and causes a biphasic disease consisting of early acute (polio)encephalomyelitis and late chronic inflammatory demyelination. In susceptible mice, strains of the TO group establish a persistent CNS infection, which can serve as a viral model of multiple sclerosis (MS), a demyelinating disease. A cell line of RAW264.7 macrophage-like cells persistently infected with the DA strain of TMEV was previously established and named DRAW. DRAW cells can serve as an *in vitro* model of persistent TMEV infection, and may aid in the search for MS treatments.

In this thesis, using qPCR, we investigated the expression of 10 target genes in DRAW cells: *Dusp6*, *Gng12*, *Ubqln2*, *Tifa*, *Gja1*, *Prkar2b*, *Bcl2*, *Ccl5*, *Adrb2*, and *Slc7a11*. Our aim was to validate the expression of the 10 genes as previously determined by a whole-genome DNA microarray. Further, we analyzed the expression of the target genes in RAW264.7 cells newly infected with either the DA or GDVII strain of TMEV. We extracted total RNA from cultivated cell samples at sampling times  $t = 0$  h and  $t = 48$  h, reverse transcribed the RNA to cDNA, and multiplied the cDNA by qPCR. The qbase+ software was used to calculate relative expression ratios of the target genes in DRAW cells and newly infected RAW264.7 cells compared to uninfected controls, and to statistically analyze the data.

In DRAW cells, we have validated the expression of four target genes at both sampling times, and of five more target genes at one of the sampling times. Using available literature, we have gained insight into the role of the target genes in mechanisms and pathways related to TMEV infection, viral persistence, and MS. We evaluated the significance of our results in regard to these disease mechanisms. We also identified potential fields of further study regarding the roles of the particular genes within these pathways. We further noted significantly altered expression of several target genes in newly infected RAW264.7 cells and commented on the potential role of these findings in the context of early DA or GDVII strain infection.

## POVZETEK

Theilerjev virus mišjega encefalomielitisa (TMEV) je črevesni patogen miši, ki lahko povzroči tudi okužbo centralnega živčnega sistema (CŽS). Obstajata dve skupini sevov TMEV. Nevrovirulentna skupina GDVII vključuje sev GDVII in po intracerebralni inokulaciji izzove akutni encefalomielitis, večinoma s smrtnim izidom. Persistentna skupina Theiler's Original (TO) vključuje sev DA in izzove dvofazno bolezen, ki sestoji iz zgodnjega akutnega (polio)encefalomielitisa in pozne kronične vnetne demielinizacije. Sevi skupine TO v dovzetnih miših vzpostavijo trajno okužbo CŽS, ki lahko služi kot virusni model demielinizirajoče bolezni multiple skleroze (MS). Predhodno je bila vzpostavljena celična linija makrofagom podobnih celic RAW264.7, trajno okuženih z DA sevom TMEV. Ta celična linija, poimenovana DRAW, lahko služi kot *in vitro* model trajne okužbe s TMEV, morda pa lahko pripomore tudi k iskanju zdravil za uporabo pri MS.

V tej diplomski nalogi smo z uporabo kvantitativne verižne reakcije s polimerazo (qPCR) preverjali izražanje desetih tarčnih genov v DRAW celicah: *Dusp6*, *Gng12*, *Ubqln2*, *Tifa*, *Gja1*, *Prkar2b*, *Bcl2*, *Ccl5*, *Adrb2* in *Slc7a11*. Naš namen je bil validirati izražanje teh 10 genov, kot je bilo predhodno določeno z metodo DNK mikromrež celotnega genoma. Nadalje smo preverjali izražanje tarčnih genov v RAW264.7 celicah, sveže okuženih z DA ali GDVII sevom TMEV. V vseh primerih smo iz vzgojenih celičnih vzorcev pridobili celokupno RNK ob časih vzorčenja  $t = 0$  h in  $t = 48$  h. RNK smo obratno prepisali v cDNK, ki smo jo pomnožili s qPCR. S programsko opremo qbase+ smo izračunali razmerja relativnega izražanja tarčnih genov v DRAW celicah in sveže okuženih RAW264.7 celicah v primerjavi z neokuženimi celicami. Podatke smo tudi statistično obdelali.

V DRAW celicah smo validirali izražanje štirih tarčnih genov ob obeh časih vzorčenja in petih nadaljnih ob enem izmed časov vzorčenja. Z uporabo razpoložljive literature smo dobili vpogled v vlogo tarčnih genov v mehanizmi in poteh, povezanih z okužbo s TMEV, virusno persistenco in MS. Ocenili smo pomen naših ugotovitev v povezavi z omenjenimi mehanizmi in potmi ter identificirali potencialna področja nadaljnih študij za preiskovanje vloge posameznih genov znotraj njih. Opazili smo tudi značilno spremenjeno izražanje večih tarčnih genov v sveže okuženih RAW264.7 celicah in komentirali pomen teh ugotovitev v okviru zgodnje okužbe z DA ali GDVII sevom.

## LIST OF ABBREVIATIONS

ACTB	beta-actin
ADRB2	adrenergic receptor beta 2
ANOVA	analysis of variance
BCL-2	B-cell lymphoma 2
BHK-21	baby hamster kidney fibroblasts
bp	base pair
cAMP	cyclic adenosine monophosphate
CCL5	chemokine (C-C motif) ligand 5; also known as RANTES
cDNA	complementary DNA; a nucleic acid synthesized from a mRNA template in a reaction catalyzed by the enzyme reverse transcriptase
CNS	central nervous system
C <sub>T</sub>	crossing threshold; the point in PCR at which the amplification signal rises appreciably over the background signal
Cx43	connexin 43
DMEM	Dulbecco's modified Eagle medium
DNA	deoxyribonucleic acid
DUSP6	dual specificity phosphatase 6
<i>E</i>	amplification efficiency
EAE	experimental autoimmune encephalomyelitis
EDTA	ethylenediaminetetraacetic acid
ERK1/2	extracellular signal-regulated kinase 1/2
FBS	fetal bovine serum
FW	forward primer; binds to the non-coding strand of DNA and initiates DNA elongation from the 5' to the 3' end in PCR
<i>g</i>	standard gravity; the acceleration due to gravity at the Earth's surface
GAPDH	glyceraldehyde-3-phosphate dehydrogenase
GJA-1	gap junction alpha-1 protein; also known as connexin 43
GNG12	G protein, gamma-12 subunit
GPCR	G protein-coupled receptor
Hsp70	70 kDa heat shock protein
IL	interleukin

IFN	interferon
mRNA	messenger RNA
MAPK	mitogen-activated protein kinase
MMLV	Moloney murine leukemia virus
MS	multiple sclerosis
PCR	polymerase chain reaction
p.i.	post infection
PKA	protein kinase A; also known as cAMP-dependent protein kinase
PRKAR2B	protein kinase A, type II-beta regulatory subunit
qPCR	quantitative PCR
RANTES	regulated on activation, normal T cell expressed and secreted
RNA	ribonucleic acid
rpm	revolutions per minute
RQ	relative quantity
RT	reverse transcription
RT-qPCR	reverse transcription quantitative PCR
RV	reverse primer; binds to the coding strand of DNA and initiates DNA elongation from the 3' to the 5' end in PCR
SD	standard deviation
SLC7A11	solute carrier family 7 (anionic amino acid transporter light chain, $x_c^-$ system), member 11; also known as xCT
TIFA	TRAF-interacting protein with a forkhead-associated domain-containing protein A
TMEV	Theiler's Murine Encephalomyelitis Virus
TO	Theiler's Original group of Theiler's Murine Encephalomyelitis Virus strains
TRAF	tumor necrosis factor receptor-associated factor
UBQLN2	ubiquilin 2
UPS	ubiquitin-proteasome sytem

# 1. INTRODUCTION

## 1.1. Theiler's Murine Encephalomyelitis Virus

### 1.1.1. Properties

Theiler's Murine Encephalomyelitis Virus (TMEV) is a member of the *Theilovirus* species within the *Cardiovirus* genus, *Picornaviridae* family, *Picornavirales* order. Members of the *Picornaviridae* family exhibit a capsid, but no envelope, wherein one molecule of positive sense, single stranded ribonucleic acid (RNA) is enclosed. This virion RNA is infectious, 8100 base pairs (bp) in size, and serves as both the genome and the viral messenger RNA (mRNA) (1). It encodes a single polyprotein, which is cleaved into 12 mature proteins as a result of posttranslational processing, as pictured in Figure 1. In TMEV, posttranslational processing follows a standard L-4-3-4 picornavirus polypeptide arrangement: a leader protein, four proteins in part one of the genome, three proteins in part two, and four proteins in part three (2).

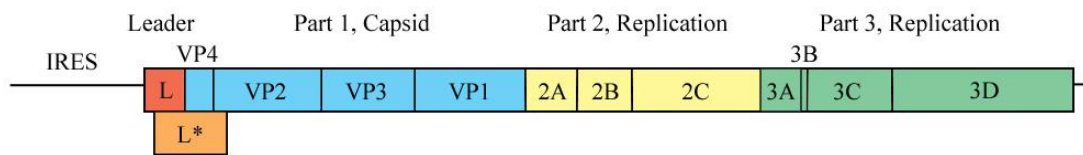


Figure 1. The TMEV genome, featuring its internal ribosome entry site (IRES). Figure adapted from Brahic *et al.* (3).

The role of the viral proteins is diverse. The leader protein, L, interferes with the innate immune response against the virus by inhibiting interferon (IFN) and cytokine gene transcription in infected cells. Multiple copies of the proteins VP1–VP4 constitute the capsid, a major determinant of viral tropism. 3C is a protease cleaving the TMEV polyprotein, 3D is the RNA-dependent RNA polymerase, and 2B, 2C, 3A and 3B are involved in genome replication as well (3).

Additionally, a protein termed L\* can be translated from an alternate open reading frame, utilizing an AUG starter codon 22 bp downstream of the AUG starter codon of the polyprotein (2). L\* may be involved in viral persistence in the central nervous system (CNS), which is discussed further below.

### ***1.1.2. Pathogenicity***

TMEV is a natural enteric pathogen of mice (4). Most picornaviruses are specific for one, or a very few host species (1), and barely one strain of the virus has been recovered from another species, namely the laboratory rat. Other rodent species were found to be positive for TMEV antibodies, although the prevalence of the infection is much lower than in wild mice (4).

The virus and its effects on mice were first described in 1937 by Max Theiler (5). TMEV commonly causes asymptomatic enteric infections in these rodents. Transmission of the virus under natural conditions is by the fecal–oral route. After enteric infection the virus can spread to the CNS, although this occurs rarely (4); TMEV, regardless of the virus strain, does not readily produce CNS disease following peripheral routes of inoculation (2). When CNS infection occurs, or the mouse is intracerebrally inoculated, the infection presents itself with neurological symptoms depending on the particular virus group and strain.

TMEV strains can be divided into two groups: the GDVII group and Theiler's Original (TO) group (2,6). Those two groups are genetically distinct (7) and differ in their neurovirulence, clinical manifestation of disease and antigenicity (8). The GDVII group also exhibits a higher virus titer post inoculation (6). During our research, we made use of two TMEV strains, GDVII and DA, as representatives of the two groups. The two strains have been sequenced and extensively studied (8).

### ***1.1.3. GDVII group and GDVII strain***

The GDVII group includes the highly neurovirulent strains GDVII, FA and ASK-1 (2). GDVII is the eponymous strain of the group. It was first observed, characterized and named by Max Theiler in 1940 (9). After intracerebral inoculation in mice, the virus replicates widely in the brain and spinal cord, where it infects neurons and glia. It induces an acute encephalitis or encephalomyelitis in which viral antigen–positive neurons and apoptotic neurons are present in the grey matter (10). The virus only infects neurons of the grey matter, and is never found in white matter (11). Clinical signs of the infection include a hunched posture and hind leg paralysis. The disease is rapidly fatal, and most animals die in 7–10 days as a result of widespread cytolytic infection wherein the virus directly kills

large numbers of neurons (2). Very few animals survive the infection, and in those that do, the virus is cleared from the CNS and does not persist (6,8).

#### ***1.1.4. Theiler's Original group and DA strain***

The TO group includes the less virulent, persistent strains DA, BeAn 8386, WW, TO4, Yale (7), and others. The DA strain was first recovered by Joan B. Daniels, who described its effects on mice in 1952 and serves as the eponym of the strain (12). After intracerebral inoculation of susceptible mice, an infection with the DA strain presents itself as a distinct biphasic CNS disease (13). The early acute phase occurs within three to 12 days post infection (p.i.) (8). An acute polioencephalomyelitis is seen, wherein neurons and a small amount of glial cells (astrocytes and oligodendrocytes) become infected (2). The distribution of infected and apoptotic neurons in the grey matter is similar to the observations in GDVII infection. The number of affected neurons in DA infection is, however, smaller (10), and destruction of neurons occurs to a variable degree (8). Clinically, hind leg paralysis appears, from which most animals recover completely (2). Despite significant reduction of viral titers, the virus is not completely cleared, but instead persists in monocytes/macrophages, microglia, astrocytes, and oligodendrocytes. The late chronic phase then follows at 30 to 40 days p.i. (8). The inflammation in the grey matter subsides (10) while inflammatory demyelinating lesions appear in the white matter (2,8). The disease leads to progressive spinal cord atrophy and axonal loss (8). This presents as gait spasticity followed by progressive clinical manifestations of neurological disability (2). The virus persists in the CNS for the lifetime of the mouse (14) and eventually causes death of the animal (8).

The course of the disease can vary slightly in infections with other strains of the TO group. In BeAn strain infection, the kinetics of the disease differ in comparison with DA infection, and the early acute phase is more attenuated (8). However, all TMEV strains in the TO group appear to be capable of establishing persistent CNS infection in susceptible mice (6).

### ***1.1.5. Viral persistence***

To establish persistence, TMEV must be able to achieve a balance between viral advances and host defenses. Therefore, to elucidate the underlying mechanisms, the cellular and viral determinants of persistence have been the subject of many studies, and have been extensively reviewed by Brahic *et al.* (3), Lipton *et al.* (15), and Oleszak *et al.* (8).

Studies investigating host genetic susceptibility to persistent infection, using various strains of mice, revealed susceptibility to be quantitative and multigenic. H2 class I genes play a major role, while additionally, several non-H2 loci influence persistence, seemingly by influencing host immune response to the virus (3).

A protein receptor on the host cell surface remains yet to be identified. However, carbohydrate co-receptors have been identified for both TMEV groups. The GDVII group appears to utilize heparan sulfate, while the TO group uses sialic acid as a co-receptor. Sialic acid binding is also required for persistence of infection with these strains. The viral capsid, which makes direct contact with the co-receptor, therefore appears to play a major role in persistence (15).

Strains of TMEV evolved mechanisms to counteract early innate immune responses, and these may consequently aid in establishing persistence. The L protein facilitates viral replication *in vivo* by inhibiting the production of IFN- $\alpha$ 4 and IFN- $\beta$  (16). It also disturbs the subcellular localization of proteins, notably including IFN regulatory factor 3 (IRF-3) (17). This disturbance may also affect cytokine and chemokine production that depends on nuclear translocation of transcription factors (3).

In mice susceptible to persistent TMEV infection, the virus persists primarily in infiltrating macrophages (18). The L\* protein is important in DA strain persistence, but is not expressed by the non-persistent GDVII group. L\* achieves an anti-apoptotic effect in macrophages, which enhances viral replication in these cells by preventing apoptosis of the viral reservoir. This effect may be mediated through interference with the anti-TMEV cytolytic T-cell response (19). Conversely, however, a review by Lipton *et al.* describes a mechanism of persistence wherein BeAn strain infected macrophages do undergo apoptosis, and thereby restrict the assembly of infectious virus. The authors argue that persistence is enabled by disallowing productive infection in these cells, and that this further enables virus spread to glia via phagocytosis in the face of immune response (15).

These contradictory findings may be due to the differences between the two virus strains DA and BeAn, the specific pathologies of their respective diseases, and/or the experimental design in each case.

Oligodendrocytes, and especially myelin, also appear to play a critical role in viral persistence. The virus found in neurons in the early phase of TMEV infection was suggested to be transported axonally, infecting myelin and spreading to oligodendrocytes (20), one of the sites of viral persistence. The infection of these cells is productive and lytic (15), resulting in demyelination. Further, mutations involving one of two myelin proteins, myelin basic protein or proteolipid protein, cause severe lack of myelin. Mice affected by either of these mutations are resistant to persistent infection (21). Given these findings, myelin may indeed be essential for viral persistence.

## **1.2. Theiler's Murine Encephalomyelitis Virus in multiple sclerosis research**

### ***1.2.1. Multiple sclerosis***

Multiple sclerosis (MS) is a chronic inflammatory disease of the CNS (22) and the most common demyelinating disease (23). In MS, focal lymphocytic infiltration leads to damage of myelin (22) which typically presents as plaques, or lesions, of the CNS white matter (23); see Figure 2. Demyelination is followed by injury to axons as well as oligodendrocytes, the myelinating cells of the CNS. All of the above results in neurological symptoms, which in the majority of cases gradually lead to disability. Clinically, the course of the disease is very variable, but will generally take one of four defined patterns. Among those, the "relapsing–remitting" pattern (acute attacks divided by periods of stability) is by far the most common (24).

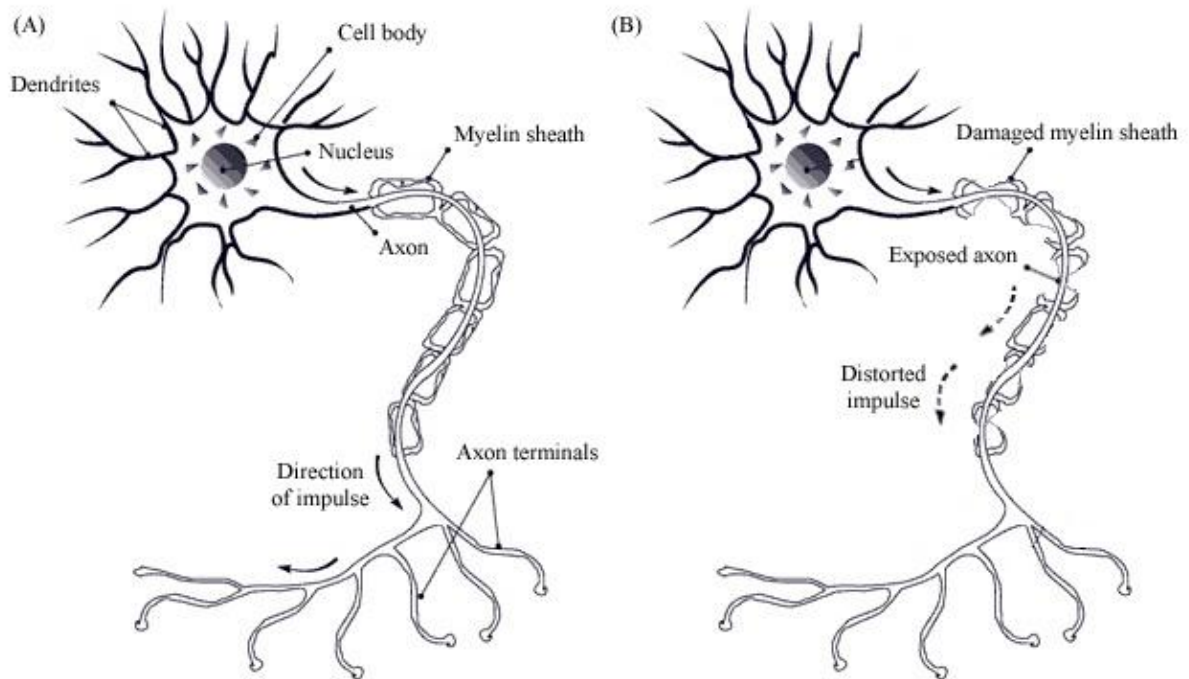


Figure 2. Schematic representation of undisturbed impulse conduction (A) and demyelination (B) in a neuron. Demyelination causes neural impulse distortion through instability or block of conduction, or by generation of ectopic impulses (24). Adapted from source (25).

MS affects about two million people worldwide. The etiology of the disease is still uncertain, but it is very likely that both genetic and environmental factors contribute to its development. Many potential environmental triggers of MS, including several viral and bacterial pathogens, have been studied, but none confirmed, despite increasing amounts of evidence suggesting one or more infectious agents as triggers of MS. In case of viral etiology, persistent infection may be responsible for demyelination and axonal injury by one of several proposed mechanisms. An autoimmune component of the disease, possibly via shared epitopes of a myelin antigen with an as of yet unknown virus, has also been hypothesized, and is supported by indirect evidence (24).

Several drugs are used to manage the course of the disease and reduce its severity, most importantly IFN- $\beta$  and glatiramer acetate (Copaxone). Despite this, no cure for MS currently exists (24). To improve existing treatments and eventually cure MS, the existence of *in vivo* and *in vitro* models of the disease is of great importance.

### ***1.2.2. Experimental models of multiple sclerosis***

Most of our current knowledge about MS has been obtained from studying animal models of the disease (26). Both *in vivo* and *in vitro* models of MS exist. The *in vivo* animal models are further divided into several types. The immune-mediated models include the most widely used, prototype MS model termed experimental autoimmune encephalomyelitis (EAE) (27), which is initially mediated by T cells and mimics MS in many aspects of pathology (24). Transgenic mouse models can be used to elucidate the pathogenic mechanisms of EAE. Further, toxin models exist, wherein substances such as ethidium bromide, lysophosphatidil cholyne, and cuprizone are used to induce toxin demyelination. These models are useful for studying demyelination and remyelination in the absence of the remaining disease factors (27).

A final category of *in vivo* models are virus-induced models of MS. These are inflammatory demyelinating diseases resembling MS. They can be triggered in different animal species by a variety of viruses (8), in rodents most notably by TMEV, Semliki Forest virus, and mouse hepatitis virus (27). The models can serve as a means of studying MS pathology while simultaneously providing a hypothetical mechanism of virus-induced autoimmunity (14). This is important due to the role viral etiology appears to play in the susceptibility of humans to MS (8).

*In vitro* models of MS include various primary cultures and cell lines that are involved in MS pathology, such as neurons, oligodendrocytes, astrocytes, and microglia. More complex *in vitro* models include spheroid and 3D CNS cultures, brain slice cultures, and blood-brain barrier models (27).

The model used in a particular research situation should address the requirements of that study. An ideal model of MS is, at present, not available, yet the existing models have various applications, and useful data continue to be obtained from them.

### ***1.2.3. TMEV persistent infection in vivo as a model of multiple sclerosis***

In 1952, Daniels first noted the demyelinating effect of the DA strain of TMEV and the persistence of virus in mouse CNS (12), but it was not until Lipton described the biphasic nature of the infection in 1975 (13) that wider interest in the demyelinating aspect of the disease was awakened. The late chronic demyelinating stage of TMEV infection in susceptible mice has been recognized as one of the best experimental animal models of MS "*because of its histopathological and immunological similarities as well as its similar genetic characteristics to MS*" (8). Several parallels between aspects of late phase TMEV infection and MS are listed below.

(1) *Neuropathology*. The neuropathologies of late phase TMEV infection and MS share the following morphological features, which can be observed in both diseases to an often variable degree:

- inflammatory infiltrates;
- perivascular inflammation;
- disruption of the blood-brain barrier;
- demyelination;
- remyelination (which is variably successful, especially in MS);
- damage to oligodendrocytes in similar patterns;
- damage to axons and the related neurological disability (8).

Additionally, apoptosis may play a role in MS pathogenesis, and was also observed in DA infection, in both the early phase (in neurons) and the late phase (in the white matter of the spinal cord) (10). Conversely, T lymphocytes in both MS and late phase DA infection may share a related impairment of the apoptotic pathway, related to *Bcl2* expression and possibly enabling demyelination (8).

It should be noted that while in late phase TMEV infection, white matter lesions primarily affect the spinal cord, in MS, they are dispersed throughout the CNS, but found more frequently in the optic nerves, brain stem, cerebellum and spinal cord (8).

(2) *Immunology*. Inflammation is a prominent feature of both MS and late phase TMEV infection, and represents the background of demyelinating processes in both diseases. In demyelinating lesions, the inflammatory infiltrates in both cases consist of T lymphocytes, monocytes/macrophages, and relatively few B lymphocytes and plasma cells. Activated microglia are present as well (8,24).

MS and late phase TMEV infection also share a related, complex cytokine response consisting of both pro-inflammatory and anti-inflammatory cytokines (8). These include interleukin 1 (IL-1), IL-2, IL-4, IL-6, IL-10, IL-12, INF- $\gamma$ , tumor necrosis factor alpha (TNF- $\alpha$ ) and transforming growth factor beta (TGF- $\beta$ ) (24,28).

Autoimmunity may be another shared feature of the two diseases. Demyelination in late phase TMEV infection is thought to be autoimmune in nature (8), as is the case in MS despite lack of direct evidence (24). A virus-induced, T-cell mediated pathogenesis of autoimmunity via molecular mimicry, or via epitope spreading, was suggested in both cases, with the autoimmune response potentially directed against various myelin epitopes (8,24).

(3) *Genetics*. Several loci of the murine genome affect genetic susceptibility of mice to TMEV infection. Viral persistence and development of the late chronic demyelinating disease are genetically controlled as well (8). Despite many difficulties in identifying associated loci, a complex genetic susceptibility also clearly contributes to the development of MS, with evidence suggesting that the phenotype of the disease is also genetically influenced (22,24).

#### ***1.2.4. TMEV persistent infection in vitro***

Compared to the studies of TMEV persistent infection *in vivo*, relatively few studies have established a persistent infection of the virus *in vitro*. Among the cells in which such an infection was successfully demonstrated are L929 cells, cerebrovascular endothelial cells, and a glioma cell line (29).

Macrophages appear to be an appropriate model to study TMEV infection *in vitro*. During late phase TMEV infection in mice, these cells have been shown to be the major site of viral persistence, as opposed to oligodendrocytes and astrocytes which are likewise infected (8,30). The virus likely enters the macrophages by infection and not phagocytosis, and active viral replication inside these cells was suggested (18). The depletion of blood-borne macrophages reportedly eliminates viral persistence and demyelination in mice (30). CNS-infiltrating macrophages were suggested to be responsible for TMEV-antigen presentation during infection (31). It has been shown that they can, together with activated microglia, also present myelin self-antigens to CD4+ T cells after the onset of myelin damage, suggesting a mechanism of active myelin targeting secondary to bystander myelin destruction. The macrophages may therefore be responsible for the induction of autoimmune pathogenesis via epitope spreading (32). Autoimmune mechanisms are thought to be "*responsible for triggering the actual demyelinating process itself*" (8), wherein macrophages may be the main effector cells for demyelination (30). They may achieve that effect by the secretion of mediators damaging to oligodendrocytes or myelin itself (8).

Given the evident importance of macrophages in TMEV infection and its persistence, *in vitro* models of TMEV macrophage infection have been established and studied in recent years. The first report of establishing a persistently DA-infected macrophage cell line has been published in 2006 by Steurbaut *et al.*, who persistently infected the RAW264.7 murine macrophage-like cell line (29), as described below. Himeda *et al.* later investigated cytokine expression in the J774.1 murine macrophage cell line persistently infected with the DA strain (33), and several other research groups have worked with TMEV-infected macrophages without investigating the persistence of infection.

### ***1.2.5. RAW264.7 macrophage-like cells***

RAW264.7 is a murine macrophage-like cell line originating from experiments by Raschke *et al.*, who derived it from a tumor induced by the Abelson murine leukemia virus. The tumor was predominantly lymphoid in nature, but contained a semi-adherent monocyte cell type. From the latter, the RAW264.7 cell line was established (34). The cell line is continuous and can therefore be subcultured indefinitely. It is available in the American Type Culture Collection which remains its major, if not sole, commercial source.

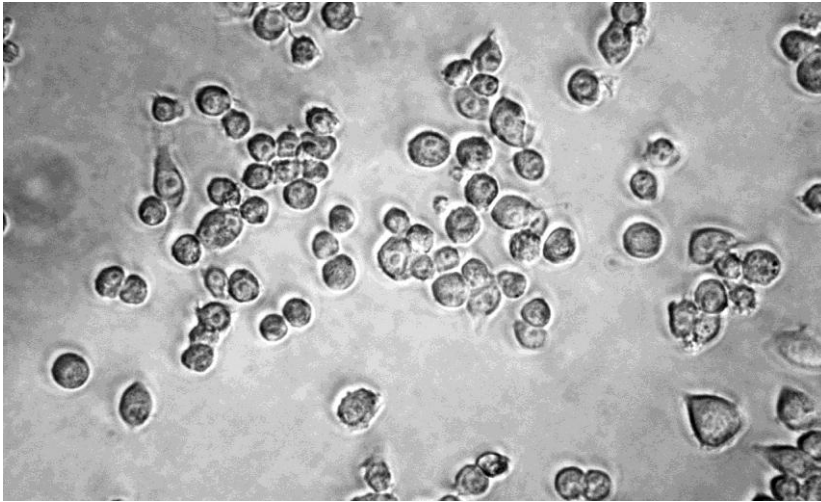


Figure 3. RAW264.7 murine macrophage-like cells. Photo courtesy of MICH.

### ***1.2.6. DRAW cells***

The DRAW cell line is a persistently infected cell line originating from experiments by Steurbaut *et al.* It is based on the persistent infection of the RAW264.7 murine macrophage-like cell line with the DA strain of TMEV. The RAW264.7 cell line was proven to support the replication of both the DA and GDVII strain of TMEV, while retaining nearly unaffected growth and cell viability. In GDVII infection, no infectious virus was found in culture as early as 5 days p.i. Conversely, the DA-infected cells continuously produced new virions, and have remained persistently infected even years p.i., thus establishing the cell line termed DRAW (29). The authors have since studied the effects of several substances on viral replication and persistence in DRAW cells (35), and examined gene expression in the cell line using a mouse whole-genome deoxyribonucleic acid (DNA) microarray (unpublished).

DRAW cells represent an *in vitro* model to study the molecular mechanism of viral persistence, directly investigate cellular and viral factors influencing the persistence of infection, and screen for potential anti-TMEV agents. Additionally, given its connection to MS, the model may aid in the search for MS treatments (29).



Figure 4. DRAW cells. Photo courtesy of MICH.

## 2. AIMS AND HYPOTHESIS

### 2.1. Aims of the thesis

MS is a demyelinating disease in which the etiology is still uncertain. Potential viral triggers have been implicated in the etiology, and persistent infection is a possible mechanism (24). Considering this, the Steurbaut *et al.* research group at the host department previously succeeded in establishing a cell line persistently infected with the DA strain of TMEV, and in cultivating it further. The cell line has been termed DRAW. It represents a first *in vitro* model to study the molecular mechanisms of viral persistence, and investigate cellular and viral factors influencing it (29).

Stimuli such as infection lead to cellular response, namely changes in expression of a number of genes in the infected cell. In our *in vitro* model, this up- and downregulation is of interest when investigating the biological processes involved in viral persistence, and potential targets to interfere with this process. With the development of DNA microarray methods, it is possible to study the global expression of all mouse genes. By comparing uninfected and infected cells, we can identify the genes that are involved in viral persistence. A whole-genome DNA microarray has previously been used at the host department to examine gene expression in DRAW cells in comparison to uninfected RAW264.7 macrophages (unpublished). However, DNA microarray findings for the most part require validation using a method with higher sensitivity, such as reverse transcription quantitative polymerase chain reaction (RT-qPCR).

The aim of this thesis is to validate the findings of the DNA microarray analysis of DRAW cells. For this purpose, we will examine the expression of ten target genes in uninfected RAW264.7 cells, as well as DRAW cells, using RT-qPCR. The choice of the target genes will be based on the interests of the host department. Involvement of the target genes in inflammation, immune mechanisms, TMEV persistence or MS is confirmed or implied in relevant literature, as referenced in § 5. (Discussion). The genes were previously shown to be significantly up- or downregulated in the DNA microarray experiments. Genes that didn't show a significant difference in expression will also be analyzed for affirmation.

The knowledge of up- or downregulation of the target genes will aid us in a better understanding of the cellular and viral molecular mechanisms of persistence, and the genes and pathways involved in it. We may also be able to provide insight into links between these pathways and MS.

Since the number of conditions that were analyzed in the DNA microarray experiments was limited to uninfected RAW264.7 cells and DRAW cells, we will introduce additional conditions when performing RT-qPCR experiments. This will include RAW264.7 macrophages, newly infected with either the DA or the GDVII strain of TMEV. Thereby, we will attempt to gain additional information about the mechanisms of viral persistence.

## **2.2. Working hypothesis**

- 1) Expression levels of the target genes validate their expression levels as previously determined by whole-genome DNA microarray.
- 2) The analysis of gene expression confirms, or disproves, the involvement and role of the target genes in the mechanisms of viral persistence.
- 3) The role of the gene products in cellular pathways may imply their involvement in the pathogenesis of MS.
- 4) The gene expression analysis of RAW264.7 cells newly infected with DA or GDVII virus highlights potential differences in the expression of the target genes between early and late phase of TMEV DA strain infection, and between the early phases of TMEV DA and GDVII strain infections in macrophages.

## 3. MATERIALS AND METHODS

### 3.1. Cell cultivation

#### 3.1.1. Materials

*TMEV, DA and GDVII strains.* Stocks of TMEV strains DA and GDVII were kindly donated by T. Michiels (Christian de Duve Institute of Cellular Pathology, Université catholique de Louvain, Belgium). The DA strain was grown in L929 cells, and the GDVII strain in baby hamster kidney–21 (BHK-21) fibroblasts. Both strains were concentrated by ultracentrifugation.

*RAW264.7 cells.* The RAW264.7 cell line used in this research was also originally received from T. Michiels (Christian de Duve Institute of Cellular Pathology, Université catholique de Louvain, Belgium). The MICH personell maintained the cell line up to the time of research.

*DRAW cells.* Steurbaut *et al.* established the DRAW cell line at MICH, as described above. The MICH personell maintained the cell line up to the time of research.

*Dulbecco's modified Eagle medium (DMEM)* (Gibco, Grand Island, NY, USA). All cells used DMEM as the growth medium. The medium contains 25 mM D-glucose, 1 mM sodium pyruvate, amino acids (including 3.97 mM L-glutamine), vitamins, inorganic salts, and an addition of phenol red as indicator. To each 500 mL flask of such commercially obtainable DMEM, we add 25 mL (5 %) of FBS and 5 mL (1 %) of PenStrep to obtain a ready-to-use medium, which we then store in a refrigerator.

*Fetal bovine serum (FBS), Certified, US origin* (Gibco, Grand Island, NY, USA). The addition of serum to cell culture media promotes cell growth and cell attachment. It contains components important for cell cultivation, such as protein, growth factors, hormones, nutrients, metabolites, lipids and minerals. FBS is one of the most widely used sera (36).

*PenStrep* (Gibco, Grand Island, NY, USA). PenStrep is an antibiotic mixture containing 10000 U/mL penicillin G and 10000 µg/mL streptomycin, added to the medium to prevent contamination by gram positive as well as gram negative bacteria (36).

### 3.1.2. Methods

*Cultivation of RAW264.7 and DRAW cells.* Both RAW264.7 and DRAW cell cultivation occurred continuously in 75 cm<sup>2</sup> cell culture flasks, incubated at 37 °C in a 5 % CO<sub>2</sub> atmosphere. We regularly observed the cells, passaged them by replacing the medium or flask when necessary, and subcultured them in fresh medium when required.

*Infection of RAW264.7 cell line with TMEV.* We prepared a RAW264.7 cell suspension in DMEM with a concentration of  $8,0 \times 10^5$  cells per mL. 1 mL of this suspension was transferred into each 25 cm<sup>2</sup> cell culture flask. The flasks were incubated for 1 hour at 37 °C in a 5 % CO<sub>2</sub> atmosphere. 10 plaque-forming units (PFU)/cell of TMEV was then added to each flask, and the flasks were again incubated for 1 hour at the same conditions.

## 3.2. Sampling

### 3.2.1. Materials

*Ethylenediaminetetraacetic acid (EDTA).* Some of the cell adhesion determinants depend on the divalent cations Ca<sup>2+</sup> and Mg<sup>2+</sup>. Therefore, EDTA as a chelating agent facilitates cell detachment (36). The composition of the EDTA solution used for this purpose is given in Table I.

Table I. Composition of EDTA solution for cell detachment; pH = 7,4.

Component	Concentration
EDTA	1.6 mM
NaCl	137 mM
Na <sub>2</sub> HPO <sub>4</sub> .12H <sub>2</sub> O	7.8 mM
NaH <sub>2</sub> PO <sub>4</sub> .H <sub>2</sub> O	1.3 mM
KCl	8.0 mM

*Buffer RLT.* Buffer RLT is a lysis buffer provided in the RNeasy Mini kit RNA extraction kit (Qiagen, Venlo, Netherlands), used for lysis of the sample cells after harvesting. The composition of the buffer is proprietary and therefore confidential. Immediately before use, 1 % of 14,3 M  $\beta$ -mercaptoethanol (Merck KGaA, Darmstadt, Germany) was added to the buffer to inactivate RNases, enzymes that can degrade RNA.  $\beta$ -mercaptoethanol irreversibly denatures RNases by reducing disulfide bonds and thereby destroying their native conformation, which is required for enzyme functionality (37).

### ***3.2.2. Cell harvesting***

RAW264.7 and DRAW cells were grown in a monolayer in DMEM until a confluent monolayer was observed. We then harvested the cells by discarding the medium, detaching the cells by incubation with EDTA at room temperature, and quantitatively transferring the cells to a Falcon tube. The tube was centrifuged for 5 minutes at  $300 \times g$  using a Sanyo Harrier 18/80 centrifuge (MSE, London, UK). The supernatant was discarded and the cell pellet resuspended in DMEM. The cells were counted using a Bürker chamber and a Orthoplan light microscope, planapochromat 16/0,40 objective (Leitz, Wetzlar, Germany).

### ***3.2.3. Starting a sampling experiment***

Taking into account the result of the cell count, we diluted the cell suspension with DMEM as required, and transferred a volume of cell suspension containing  $8,0 \times 10^5$  cells to a 25 cm<sup>2</sup> cell culture flask. Then, the sampling experiment was started (see Figure 5). All samples ran in triplicate. For the duration of the experiment, the medium remained unreplaced in order to limit external influences on samples.

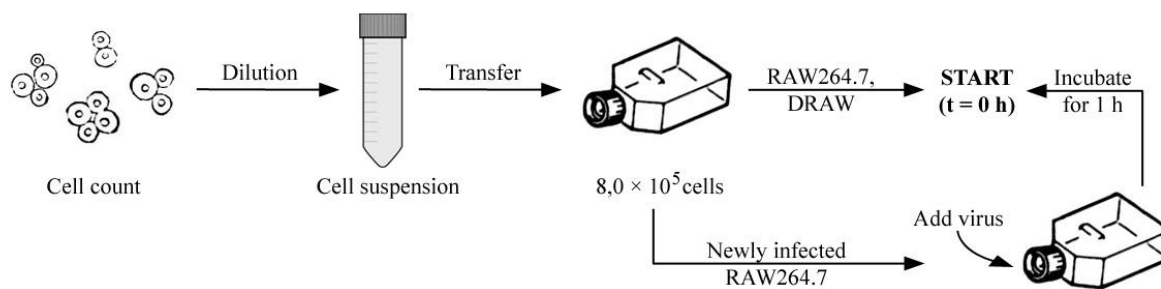


Figure 5. The starting point of the experiment ( $t = 0$  h). For RAW264.7 and DRAW cells, the start of the experiment is the point of transferring the cell suspension to the cell culture flask. For the newly infected RAW264.7 cells, the start of the experiment is the point one hour p.i., after incubation at  $37^\circ\text{C}$  in a 5 %  $\text{CO}_2$  atmosphere.

### 3.2.4. Sampling

For all cells, sampling occurred at two time points: immediately at the start of the experiment ( $t = 0$  h) and after 48 hours of incubation at  $37^\circ\text{C}$  in a 5 %  $\text{CO}_2$  atmosphere ( $t = 48$  h). These two time points were chosen since the gene expression was also previously determined at these times with the use of a DNA microarray.

At  $t = 0$  h, the cell suspension was collected. At  $t = 48$  h, the medium was collected, and the cells were harvested by incubation with EDTA at room temperature, followed by combining the medium and the harvested cells in EDTA.

After sampling, a volume of  $200\ \mu\text{L}$  of each sample was removed for characterization. The remaining cell suspension was centrifuged for 5 minutes at  $300 \times g$ . After discarding the medium, resuspension of the cell pellet in the required volume of lysis buffer followed (see Table II). We stored the lysed cell suspension at  $-80^\circ\text{C}$  until RNA extraction.

Table II. Volume of Buffer RLT for cell lysis depending on the number of pelleted cells. The upper limit of  $1 \times 10^7$  cells represents the uppermost number of cells that can be processed as a single sample during RNA extraction.

Number of pelleted cells	Volume of Buffer RLT [ $\mu\text{L}$ ]
$< 5 \times 10^6$	350
$5 \times 10^6 - 1 \times 10^7$	600

### 3.3. Sample characterization

#### 3.3.1. Cell viability assay

We assessed the metabolic activity of cells in the harvested samples using the CellTiter-Blue cell viability assay (Promega, Madison, WI, USA). The assay is based on reduction of the indicator dye resazurin into resorufin, an ability which only viable cells retain (see Figure 6). Resorufin is highly fluorescent; the recorded fluorescence represents a measure of cellular metabolic activity and is proportional to the number of viable cells (38).

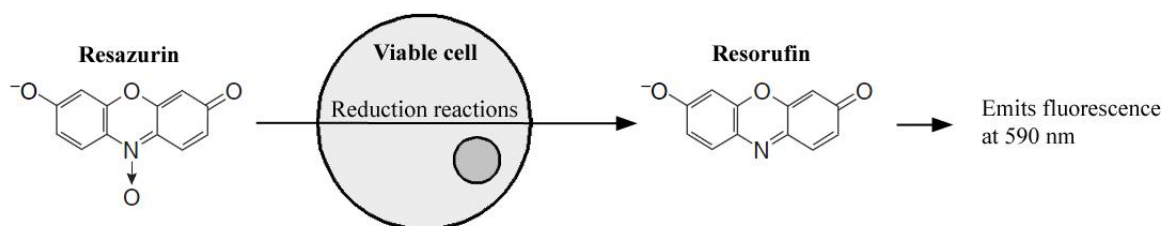


Figure 6. The reduction of resazurin to resorufin. Adapted from source (38).

To 200  $\mu\text{L}$  of cells in suspension, 40  $\mu\text{L}$  CellTiter-Blue reagent was added. The samples were incubated for 2 hours in separate wells of a 96-well plate, at 37  $^{\circ}\text{C}$  in a 5 %  $\text{CO}_2$  atmosphere. Then, a FL600 microplate fluorescence reader (BioTek, Winooski, VT, USA) recorded the emitted fluorescence.

### **3.4. Total RNA extraction with DNase digestion**

#### ***3.4.1. Materials***

We extracted total RNA from all samples using the RNeasy Mini kit (Qiagen, Venlo, Netherlands) according to the manufacturer's instructions (RNeasy Mini Handbook, fourth edition, September 2010). The procedure included a DNase digestion step to eliminate potential leftover DNA using the RNase-free DNase set (Qiagen, Venlo, Netherlands). All buffers, other solutions, columns and collection tubes used are supplied in the respective commercially obtainable kits. The compositions of the buffers are proprietary and therefore confidential.

Other materials:

- 70 % ethanol, prepared by diluting absolute ethanol with nuclease-free water;
- absolute ethanol, analytical grade;
- nuclease-free water (Ambion, Austin, TX, USA).

#### ***3.4.2. Protocol***

The previously lysed cell samples were homogenized by vortexing for 2 minutes. Then, one volume of 70 % ethanol was added, and the sample was mixed well by pipetting. The mixture was transferred to a spin column placed inside a 2 mL collection tube. The extraction was performed according to the protocol in Table III. A schematic representation of the protocol is featured in Figure 7.

Table III. Total RNA extraction protocol. In case volume of the sample and ethanol mixture exceeded 700  $\mu\text{L}$ , it was centrifuged at the same column in two parts, the first equaling 700  $\mu\text{L}$  and the second part the remaining volume.

	<b>Component added to column</b>	<b>Volume [ml]</b>	<b>Centrifugation</b>
1.	Sample + 70 % ethanol	Total, $\leq 700 \mu\text{L}$	$\geq 10\,000$ rpm, 15 s
2.	Washing buffer RW1	350 $\mu\text{L}$	$\geq 10\,000$ rpm, 15 s
3.	10 $\mu\text{l}$ DNase I + 70 $\mu\text{l}$ buffer RDD	80 $\mu\text{l}$	Incubate at room temperature, 15 min
4.	Washing buffer RW1	350 $\mu\text{L}$	$\geq 10\,000$ rpm, 15 s
5.	Washing buffer RPE	500 $\mu\text{L}$	$\geq 10\,000$ rpm, 15 s
6.	Washing buffer RPE	500 $\mu\text{L}$	$\geq 10\,000$ rpm, 2 min
7.	Place column in new 2 mL collection tube		Full speed, 1 min
8.	Nuclease-free water	30 $\mu\text{l}$	$\geq 10\,000$ rpm, 1 min

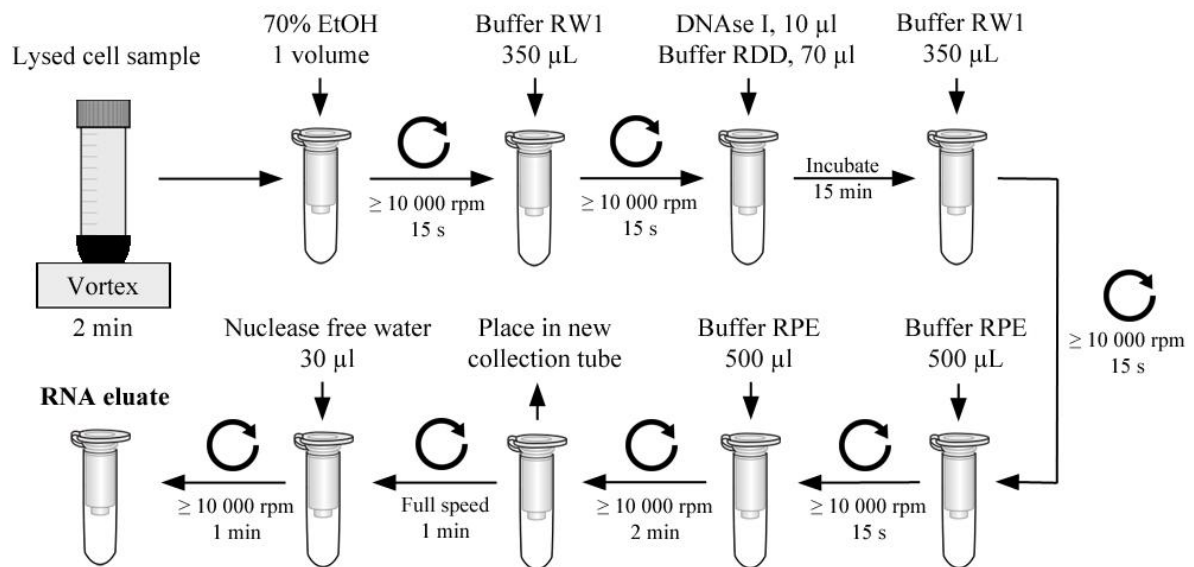


Figure 7. A schematic representation of the total RNA extraction protocol. The circular arrow represents a centrifugation step.

We eluted sample RNA in 30  $\mu\text{l}$  nuclease-free water, followed by measuring RNA concentration and assessing RNA purity (indicated by A260/A280 and A260/A230 ratios) using a Nanodrop ND-1000 Spectrophotometer (Thermo Scientific, Waltham, MA, USA). The extracted total RNA was stored at  $-80\text{ }^{\circ}\text{C}$  until use. Immediately before use, RNA concentration was remeasured using the spectrophotometer and diluted to a concentration of 6,25  $\text{ng}/\mu\text{L}$  for use in reverse transcription (RT).

### **3.5. Reverse transcription real-time quantitative polymerase chain reaction**

#### ***3.5.1. Method background***

Accurate analysis of gene expression is important in understanding gene and protein functions. To obtain information about gene expression levels, mRNA levels in examined cells must be accurately determined. This can be achieved by subjecting RNA samples to RT followed by real-time quantitative polymerase chain reaction (qPCR) (39).

To perform polymerase chain reaction (PCR) which amplifies DNA, the isolated RNA must first be converted to complementary DNA (cDNA) by RT (39). RT is a process carried out by reverse transcriptases, RNA-dependent DNA polymerase enzymes that make possible the synthesis of DNA complementary to an mRNA template. The synthetic DNA prepared in this manner is called cDNA (40). cDNA is then amplified by PCR.

PCR is a highly sensitive *in vitro* method used for amplification of a target DNA sequence. It was invented by Kary Mullis in 1983 (40), with the first research paper describing it published in 1985 (41). Today, PCR is a widely used, routine laboratory technique (39).

PCR consists of three basic temperature-controlled steps, usually repeated between 25 and 40 times:

- denaturation of template DNA at a temperature of 90–96 °C;
- annealing of replication primers to the template DNA at a temperature dependent on the primers used;
- DNA synthesis by a thermostable DNA polymerase, typically at 72 °C (39).

The replication primers are carefully designed synthetic oligonucleotides that define the ends of the template segment to be amplified. They are extended by the DNA polymerase in the third step of the reaction (40). The resulting PCR amplification products are called amplicons.

If the PCR is performed in a way that allows quantification of mRNA levels, it is termed quantitative PCR (qPCR). qPCR today represents the method of choice for analyzing gene expression of a moderate number of genes (42). However, conventional qPCR methods detect only the final end product of the amplification (39), and such end point analysis is not reliably quantitative due to the reaction reaching a plateau phase (42). To surpass this limitation, real-time qPCR was developed.

Real-time qPCR, an advance in qPCR, allows monitoring of the amplicon accumulation during each PCR cycle. Amplicon accumulation is detected and quantified in "real time" using a fluorescent detector molecule which only fluoresces when associated with the product amplicon. The recorded fluorescence is therefore directly proportional to the amount of amplicon in the reaction. The quantification of the initial amount of starting template with real-time qPCR is sensitive and reproducible (39).

Combining RT with real-time qPCR allows for amplification and relative quantification of target mRNA, and therefore gene expression (42). In our case, this method was used to provide insight into the relative gene expression levels in response to an external stimulus, namely viral infection (39).

Relative quantification is a quantification strategy in real-time RT-qPCR which measures the relative change in mRNA expression levels. It normalizes the expressed levels of target genes to one or more reference genes, often housekeeping genes. A relative expression ratio of the target gene in the test sample compared to the control sample is then calculated. Relative quantification assumes that reference gene expression is stable and unregulated, even in experimental conditions imposed upon the test samples. It requires no calibration curve, and no units to express relative quantities (43).

An RT-PCR can be performed as a one-step or a two-step reaction. In the two-step technique, which we have used, the RT and PCR steps are performed in separate tubes. This enables the use of random primers in the RT step and the creation of a cDNA pool which can then be used to amplify several target amplicons (44).

Hot-start is a method employed in PCR to avoid unwanted non-specific primer/template and primer/primer annealing prior to the start of the reaction that can occur in the reaction mixture at temperatures below 65–70 °C (39). One method of performing hot-start PCR is the use of chemically modified enzyme, such as FastStart Taq DNA Polymerase. Blocking groups restrict activity of such a thermostable recombinant *Taq* polymerase up to 75 °C. The enzyme requires a pre-incubation step (95 °C, 10 min) at the start of the experiment, ensuring temperatures at which primers no longer bind non-specifically (45).

### 3.5.2. Materials

24 total RNA samples:

- four RAW264.7 cell variants: RAW264.7 cells, DRAW cells, RAW264.7 cells newly infected with TMEV, DA strain, and RAW264.7 cells newly infected with TMEV, GDVII strain;
- two sampling points: t = 0 h and t = 48 h;
- all samples run as biological triplicates.

Each of these RNA samples was amplified in the PCR with the primer set for each tested gene, 12 in total (10 target genes and 2 reference genes). Each of these reactions was carried out in technical duplicates to ensure consistency and reproducibility of the results (39), adding up to a total of 576 single reactions (see Equation 1 and Figure 8).

Equation 1. The calculation of the total number of single PCR reactions performed.

$$n = (4 \text{ cell variants}) \times (2 \text{ sampling points}) \times (3 \text{ biological triplicates}) \\ \times (12 \text{ primer sets}) \times (2 \text{ technical duplicates}) = 576 \text{ reactions}$$

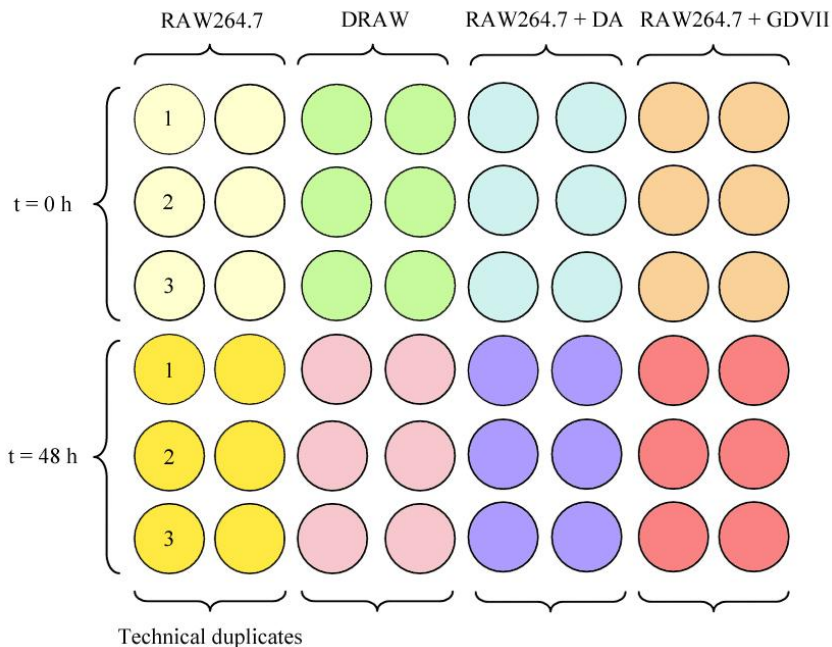


Figure 8. A schematic representation of all PCR reactions performed for each target gene. The numbers 1, 2 and 3 designate the biological triplicates of each cell variant at each sampling time. A total of 12 such reaction sets was performed.

*LightCycler FastStart DNA Master SYBR Green I kit* (Roche Applied Science, Penzberg, Germany):

- LightCycler FastStart reaction mix SYBR Green I, 10x conc. Contains reaction buffer, deoxyribonucleotide triphosphate (dNTP) mix, SYBR Green I dye and 10 mM MgCl<sub>2</sub>; without *Taq* polymerase;
- FastStart *Taq* DNA Polymerase, a chemically modified form of thermostable recombinant *Taq* polymerase (45) for use in hot-start PCR;
- MgCl<sub>2</sub>, 25 mM.

The reaction mix contains the intercalating dye SYBR Green I which enables the detection of amplicon during real-time qPCR. The dye binds to the double-stranded DNA of the PCR product, and its emitted fluorescence is greatly enhanced upon binding. The emitted signal is then recorded by the thermal cycler (39,42).

*EuroScript Reverse transcriptase, 50 U/μl* (Eurogentec, Seraing, Belgium)

EuroScript is a Moloney murine leukemia virus (MMLV) H<sup>-</sup> reverse transcriptase, a genetically modified form of MMLV reverse transcriptase. A point mutation inhibits endogenous RNase activity of the enzyme, allowing for efficient copying of longer mRNAs (39). MMLV H<sup>-</sup> is the enzyme of choice for many quantitative applications, and its cDNA synthesis rate is up to 40 times greater than that of avian myeloblastosis virus (AMV) reverse transcriptase, another common RT enzyme (43).

*Other materials:*

- ReadyMade Random Hexamer (Integrated DNA Technologies, Leuven, Belgium)
- Specific primers (Integrated DNA Technologies, Leuven, Belgium)
- RNase inhibitor, 40 U/μl (Eurogentec, Seraing, Belgium)
- Nuclease-free water (Ambion, Austin, TX, USA)

### **3.5.3. Equipment**

*MyCycler compact thermal cycler* (Bio-Rad Laboratories, Hercules, CA, USA)

*LightCycler version 1.5* (Roche Applied Science, Penzberg, Germany):

- LightCycler air cycler apparatus;
- LightCycler software version 3;
- LightCycler glass capillaries, 20  $\mu$ L.

*MultiPROBE II PLUS Liquid Handling System* (PerkinElmer, Wellesley, MA, USA). The operating protocol for the liquid handling system was programmed by Dr. Peter Kronenberger at Erasmushogeschool Brussel using WinPREP automation software.

### **3.5.4. Primer design**

We used random hexamers as primers in the RT reaction. The primers were dissolved in nuclease-free water and diluted to 50 nM with the same solvent.

Specific primers were used in the PCR. We designed the primers using the Roche LightCycler Probe Design Software and gene sequence information gathered from the National Center for Biotechnology Information (NCBI) Gene data bank (<http://www.ncbi.nlm.nih.gov/gene>). Once synthesized, we dissolved the primers in nuclease-free water and diluted them to the required concentrations with the same solvent. Sequences of the specific primers are shown in Table IV.

Table IV. Sequences of the specific forward (FW) and reverse (RV) primers used in the RT-PCR. Also included are primer positions within the gene.

<b>Gene</b>	<b>Primer</b>	<b>Sequence (5' → 3')</b>	<b>5' position</b>	<b>3' position</b>
<i>Dusp6</i>	FW	TCCCTGAGGCCATTTCTTT	1276	1294
	RV	CTTAACAATGTCGTAAGCATCG	1433	1412
<i>Gng12</i>	FW	TCAAAGATGTCCAGCAAGACG	263	283
	RV	TCCGGGCATGCTCCTCA	413	397
<i>Ubqln2</i>	FW	TGAACAACCCAGATATAATGAGGC	929	952
	RV	GCATAGGTTCTTGAATGTCAGTG	1093	1071
<i>Tifa</i>	FW	GAGTAGTTCGGCCTTTCAGATAA	322	345
	RV	CATGCAGGACACTCCGT	480	464
<i>Gja1</i>	FW	CTTCAGCCTCCAAGGAGTTC	158	177
	RV	GAGCACCGACAGCCACA	319	303
<i>Prkar2b</i>	FW	GCGTTCAACGCTCCAGTTATAAA	489	511
	RV	GCAAGCCTCTTGCAATCT	638	621
<i>Bcl2</i>	FW	GGAGCACTTTCATGTAGTTCAAGTA	5335	5359
	RV	CCTTTCCTAGACCCAGCAAT	5491	5471
<i>Ccl5</i>	FW	ATCTTGCAAGTCGTGTTTGT	233	251
	RV	GCTAGGACTAGAGCAAGCAAT	397	377
<i>Adrb2</i>	FW	CATAATCTCCTTGGCGTGT	420	438
	RV	AACTCGCACCAGAAGTTG	530	513
<i>Slc7a11</i>	FW	TGTCCTATGCAGAATTAGGTACAAG	636	660
	RV	ATGTAGCGTCCAAATGCC	801	784
<i>Gapdh</i>	FW	CATGGCCTTCCGTGTTC	3040	3056
	RV	GAAGAGTGGGAGTTGCTG	3312	3295
<i>Actb</i>	FW	CGGCCAGGTCATCACTATT	811	829
	RV	AATGTAGTTTCATGGATGCCAC	915	894

### 3.5.5. Reverse transcription

Random hexamers were used as primers in the RT reaction, and a cDNA pool was synthesized to circumvent the high inter-assay variations that can occur in RT due to different synthesis efficiencies. After the reaction, the cDNA pool was split and used in the different target-specific PCR assays, making them directly comparable (43).

The RT reaction mixture was prepared by mixing the components listed in Table V. Required amounts of the mixture were added into separate wells of a PCR plate. Into each well, extracted total cytoplasmic RNA from one of the samples, previously diluted to 6.25 ng/ $\mu$ L, was also added. The volume of the RNA solution added was equal to the volume of the reaction mixture already contained in the well. The starting amount of RNA for starting a single reaction is calculated in Equation 2.

Equation 2. The starting amount of RNA for a single reaction.

$$m = \gamma \times V = 6.25 \frac{ng}{\mu L} \times 4 \mu L = 25 \text{ ng}$$

Table V. Components of the RT reaction mixture. Noted are the amounts required for carrying out a single PCR reaction ( $V_{\text{single}}$ ) as well as the total volume required for all 576 reactions ( $V_{\text{total}}$ ).

Component	$V_{\text{single}}$ [ $\mu$ L]	$V_{\text{total}}$ [ $\mu$ L]
LightCycler FastStart reaction mix SYBR Green I	0.8	460.8
MgCl <sub>2</sub> , 25 mM	0.64	368.64
Nuclease-free water	1.92	1105.92
RNAse inhibitor, 40 U/ $\mu$ l	0.08	46.08
Reverse transcriptase, 50 U/ $\mu$ l	0.16	92.16
Random hexamers, 50 $\mu$ M	0.4	230.4
<b>Total</b>	<b>4</b>	<b>2304</b>

To perform the RT reaction, the PCR plate with reaction mixtures was run in the MyCycler thermal cycler with the following program:

- 1) reverse transcription: incubation at 46 °C for 15 min;
- 2) inactivation of reverse transcriptase: at 95 °C for 1 min;
- 3) cooling.

After the reaction, we divided the cDNA samples into single-use aliquots and stored them at –20 °C until prompt use in the PCR.

### 3.5.6. Real-time quantitative polymerase chain reaction

Since we used specific primers in the amplification of the investigated amplicons, we prepared the PCR mix separately for each primer set. The mix was prepared by manually combining the components listed in Table VI in a microcentrifuge tube. A protocol adapted from the Roche LightCycler FastStart DNA Master SYBR Green I kit manual was used.

Table VI. Components of the PCR reaction mixture. Noted are the amounts required for carrying out a single PCR reaction as well as the total volume required for each primer set (48 reactions). 4 µL out of the 4.5 µL for a single PCR reaction was pipetted into each tube of a PCR plate by the liquid handling system.

Component	V <sub>single</sub> [µL]	V <sub>total</sub> [µL]
LightCycler FastStart reaction mix SYBR Green I	0.4	19.2
MgCl <sub>2</sub> , 25 mM	0.32	15.36
Nuclease-free water	2.42	116.16
Forward primer, 20 µM	0.6	28.8
Reverse primer, 20 µM	0.6	28.8
LightCycler FastStart enzyme ( <i>Taq</i> polymerase)	0.16	7.68
<b>Total</b>	4.5	216

The cDNA samples were manually distributed into the wells of a PCR plate. The liquid handling system then distributed the PCR mix into the relevant wells. After mixing, the liquid handling system transferred the complete reaction mixture into glass capillaries. Those were then sealed and transferred to the LightCycler air cycler, where the program detailed in Table VII was run to perform the PCR reaction.

Table VII. The LightCycler program used to perform PCR on the cDNA samples.

<b>Program</b>	<b>Target temperature [°C]</b>	<b>Hold time [s]</b>	<b>Slope [°C/s]</b>	<b># of cycles</b>
<b>Hot start</b>	95	600	20	1
<b>PCR</b>	<b>1. Denaturation</b>	95	10	40
	<b>2. Annealing</b>	60	10	
	<b>3. Synthesis</b>	72	10	
<b>Melting curve</b>	95	0	20	1
	65	60	20	
	95	0	0.1	
<b>Cooling</b>	45	0	20	1

The PCR progress was monitored in real time using the LightCycler software. After the reaction, the capillaries containing the amplified samples were collected and stored at  $-20^{\circ}\text{C}$ .

### ***3.5.7. Optimization***

Prior to carrying out our experiments, we carefully designed the experimental protocol to ensure optimal reaction conditions and exclude potential disturbances and errors.

We evaluated all primers by preliminary use in the qPCR protocol. The resulting amplification of test RNA samples was evaluated, and where necessary, new primers were ordered. The sequences seen in Table IV (§ 3.5.4.) represent the final primer selection.

We also evaluated the use of the liquid handling system and selected the pipetting steps in which to use it. We adapted and optimized the working protocol of the liquid handling system to suit our pipetting needs.

Further, we designed the practical protocol for all reactions in a way that minimized the exposure of samples and reaction mixes to room temperature, as well as to any potential contaminants.

### ***3.5.8. Control reactions***

In general, two kinds of controls are introduced in RT-qPCR experiments to avoid overestimation of the fluorescence signal. Parallel to RT of samples, reactions for each sample without the use of RT enzyme are performed. These are termed "RT negative controls" and are used to verify the absence of genomic DNA contamination (43). Parallel to qPCR runs, reactions for each PCR mix without the use of cDNA template are performed. These are termed "no template controls" and are used to verify the absence of external DNA contamination of the reaction mix (44,46).

In our experimental design, we did not account for these controls. However, during RNA extraction, we have minimized DNA contamination by incorporating treatment with RNase-free DNase. The enzyme itself was washed from the extraction column afterwards and therefore removed from the sample (43). Further, specific primers for the majority of tested genes (8 out of 12) were chosen to also span or flank exons, and so using these primers, genomic DNA cannot be transcribed due to the presence of introns. And lastly, RT negative controls have been performed in preliminary experiments testing primer suitability, using RNA samples extracted in the same way as proper samples. The controls were negative for DNA contamination at all times, although this clearly cannot be extrapolated to future samples.

### 3.6. Data analysis

To obtain accurate information about gene expression in investigated cells, we mathematically and statistically analyzed the data obtained from the qPCR.

#### 3.6.1. Amplification efficiency

In theory, 100 % PCR efficiency represents the doubling of the template DNA amount in each PCR cycle. In practice, PCR is not 100 % efficient (39), and Pfaffl notes that "*efficiency evaluation is an essential marker in real-time gene quantification procedure*". It is therefore important to determine the amplification efficiencies of target and reference genes before the start of normalized gene expression calculation (43). We calculated amplification efficiencies for all samples using LinRegPCR software.

LinRegPCR is a program based on a method described by Ramakers *et al.* It utilizes data from amplification plots of PCR reactions monitored using fluorescent dyes such as SYBR Green I. The program determines the log-linear part of the data by selecting a window of linearity. Within its limits, it employs linear regression, and then calculates the intercept and the slope of the linear regression line. The intercept is used to calculate the starting concentration per sample, expressed in arbitrary fluorescence units (see Figure 9) (47). PCR efficiencies per sample are calculated from the slope using Equation 3.

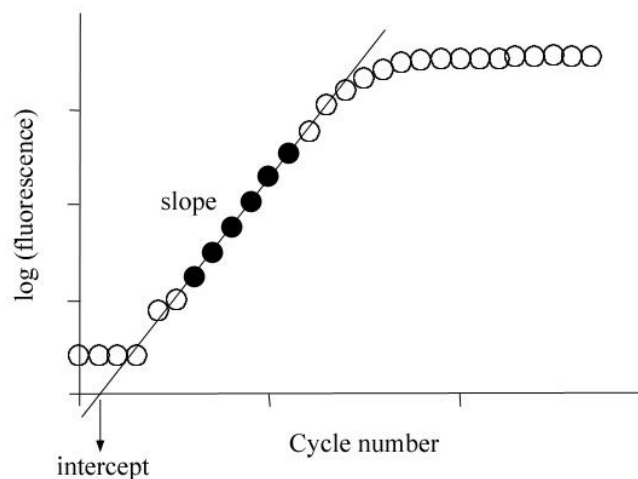


Figure 9. Log fluorescence values plotted against cycle number. Black circles represent data points included in the window of linearity. The linear regression line is shown, including slope and intercept. Adapted from Ramakers *et al.* (47).

Equation 3. Calculation of amplification efficiency from slope.  $E$  = amplification efficiency.

$$E = 10^{[-1/slope]}$$

### 3.6.2. Relative quantification

To investigate the expression of our genes of interest, we employed relative quantification of target gene transcripts to two reference gene transcripts. We analyzed the raw qPCR data using the qbase+ software (Biogazelle, Ghent, Belgium), and used it to determine the relative expression ratios of the target genes in the test samples compared to the control sample. DRAW cells, as well as RAW264.7 cells newly infected with either the DA or GDVII strain of TMEV, represented the three test samples, while the RAW264.7 cell line represented the control sample.

Using the qbase+ software, we mathematically analyzed the data using the  $\Delta\Delta C_T$  model (also named the Livak model after its author). The  $\Delta\Delta C_T$  model is a relative quantification model without efficiency correction, and assumes a static amplification efficiency of 100 %,  $E = 2$ . The relative quantities (RQs) of target genes are calculated using Equations 4–6 (43).

Equations 4–6. The  $\Delta\Delta C_T$  model for the calculation of the RQs of target genes in the test sample compared to the control sample.  $C_T$  = crossing threshold.

$$RQ = E^{-[\Delta C_{T\ test} - \Delta C_{T\ control}]} = 2^{-[\Delta C_{T\ test} - \Delta C_{T\ control}]} = 2^{-\Delta\Delta C_T}$$

$$\Delta C_{T\ test} = C_{T\ test}^{target} - C_{T\ test}^{reference}$$

$$\Delta C_{T\ control} = C_{T\ control}^{target} - C_{T\ control}^{reference}$$

It should be noted that a disadvantage of assuming a 100 % qPCR efficiency is the significant influence that small changes in amplification efficiency can have on the calculated expression ratio (43). However, we evaluated the obtained amplification efficiencies as consistent and comparable, which justifies the use of the  $\Delta\Delta C_T$  model.

The RQ values were normalized to two reference genes. As it is now known that housekeeping gene expression is never absolutely constant, but can instead vary depending on experimental conditions, normalization to multiple reference genes is preferable to normalization to a single reference gene. The common and widely used housekeeping genes *Gapdh* and *Actb* served as reference genes (43). Normalization was performed using the qbase+ software, which utilizes the geNorm algorithm to calculate the gene expression normalization factor, and normalizes the RQs to multiple reference genes (48).

### ***3.6.3. Statistical data analysis***

The data were statistically analyzed with the qbase+ software using the one-way analysis of variance (ANOVA) test. One-way ANOVA is a standard parametric test, and is commonly used to compare the equality of two or more means of groups of measurement data. The test uses one nominal variable and one measurement variable. For each nominal value, the mean of a group of measurements is calculated, and the variance among these means is compared to the variance within each group (49). The validity of one-way ANOVA relies on the assumptions that the sample populations exhibit a normal distribution, that the samples are independent, and that the variances of the populations are equal (50).

### 3.6.4. Melting curve analysis

SYBR Green I is a non-specific detection method, and the dye binds to any DNA double strand. Therefore, it does not discriminate between the desired amplicon and non-specific amplification products. One type of such non-specific products are primer-dimers, which occur due to primer extension on itself or on the opposite primer (39). To eliminate overestimation of the fluorescence signal due to non-specific products, we performed a melting curve analysis of each PCR product immediately after amplification. We visualized the melting curves using the LightCycler data analysis software.

The melting curve analysis was performed after 40 PCR cycles. The sample was briefly heated back to 95 °C, cooled it to 65 °C, and gradually heated again to 95 °C (see § 3.5.6., Table VII). During sample heating, double-strand dissociation occurs, the SYBR Green I dye is released, and therefore a fall of the fluorescence signal can be observed in real-time. A plot of fluorescence versus time is obtained during this analysis. From it, a graph of the negative first derivative of the fluorescence ( $-dF/dt$ ) versus time is constructed. In that graph, pure and homogeneous PCR amplicons produce a narrow, sharply defined peak at a higher temperature. In contrast, primer dimers produce an additional, broader peak at a lower temperature (see Figure 10) (43).

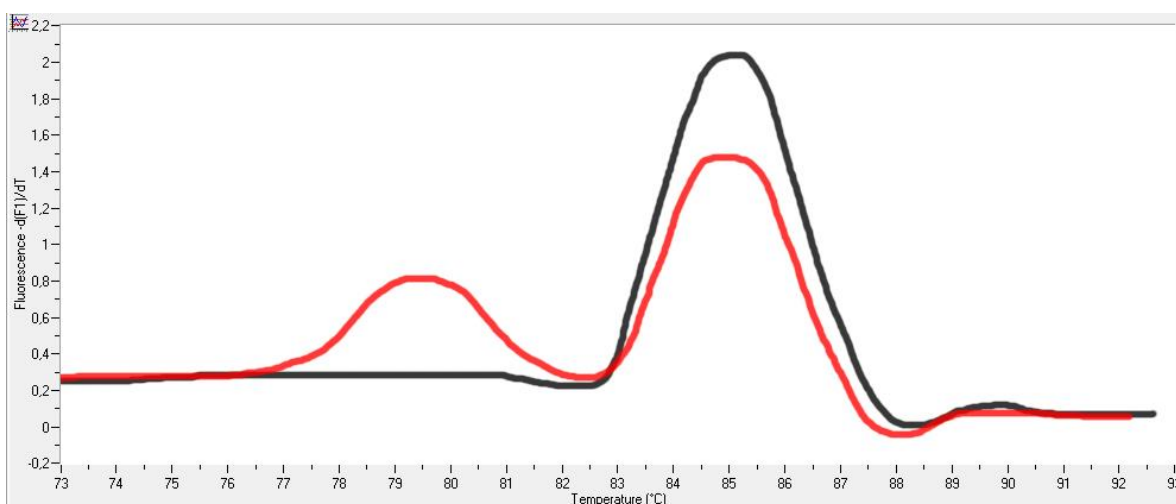


Figure 10. Schematic representation of a melting curve plot, featuring the melting curve of a pure PCR product (black) and the melting curve of a PCR product in the presence of primer dimer amplification (red). Amplification of the non-specific product occurs at the expense of specific amplification, which is diminished; note the smaller size of the specific amplicon peak.

## 4. RESULTS

### 4.1. Cell viability

The cell viability of RAW264.7 cells, DRAW cells, and RAW264.7 cells freshly infected with the DA or GDVII strain of TMEV was measured at time  $t = 0$  h and  $t = 48$  h. The results are summarized in Figure 11. The recorded fluorescence is proportional to the number of viable cells.

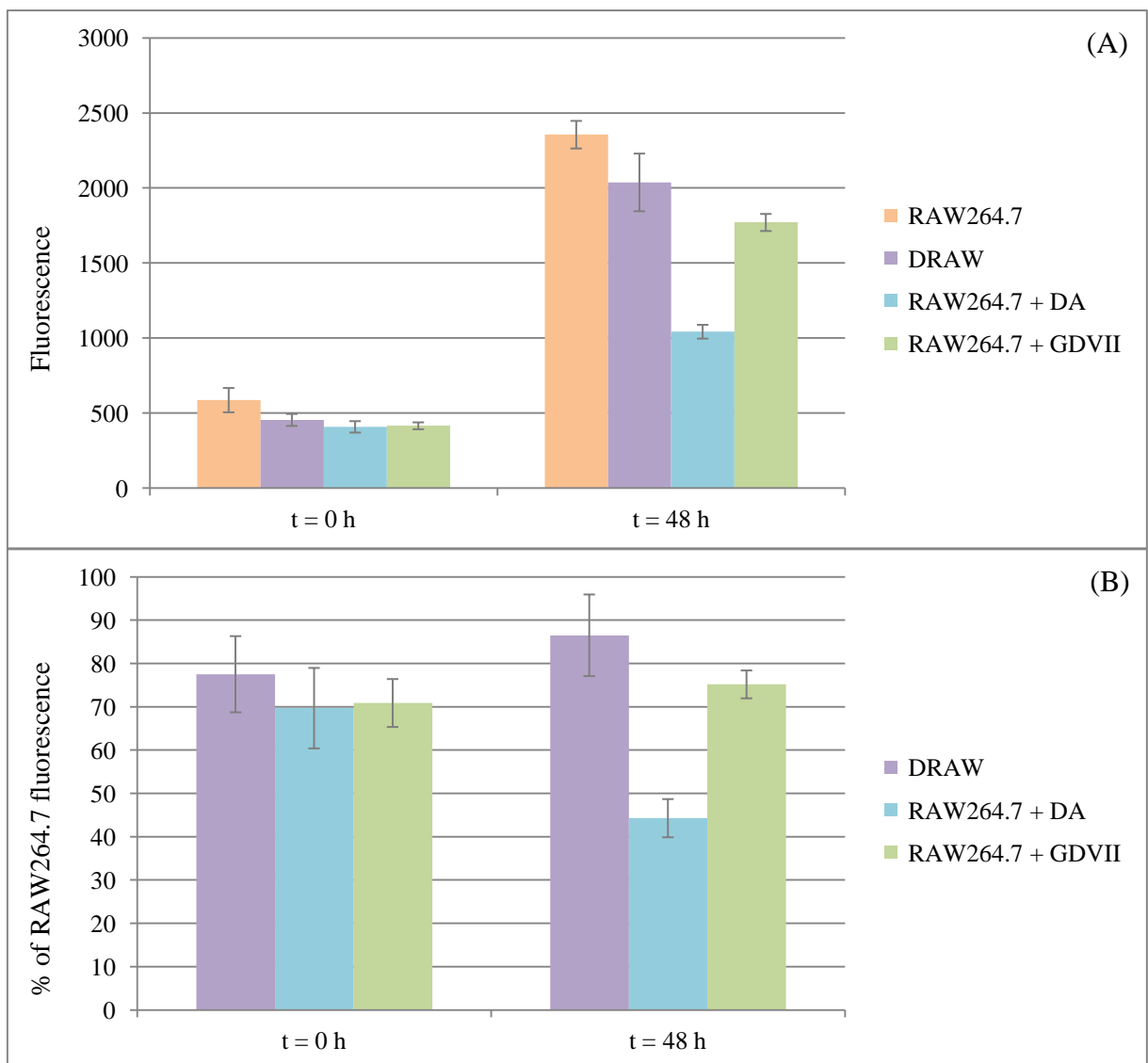


Figure 11. Cell viability (A) and cell viability expressed as the percentage of RAW264.7 cell viability (B) at points  $t = 0$  h and  $t = 48$  h. The data are presented as the mean  $\pm$  standard deviation (SD) (A), or as mean  $\pm$  relative standard deviation (RSD) (B).

The number of viable cells appears to be comparable between all four cell types at  $t = 0$  h. At  $t = 48$  h, RAW264.7 cells exhibit the highest number of viable cells, followed by DRAW cells, which appear to grow in the presence of persistent infection. Both newly infected cells exhibit a lower fluorescence, possibly due to the cytopathic effects of the newly added virus.

#### 4.2. RNA extraction

We attempted to ensure RNA quality in the process of extraction by using the Qiagen RNeasy Mini kit and following the manufacturer's suggested protocol. Use of such a column-based commercially obtainable kit should minimize carryover of potential inhibitors and other contaminants, and minimize genomic DNA contamination by including an RNase-free DNase I digestion step in the protocol.

As a preliminary testing of extracted total RNA quality, we recorded absorbance spectra of all samples. The absorbance maximum of nucleic acids lies at 260 nm, whereas absorbances at 280 nm and 230 nm represent proteins and other contaminants, respectively. RNA quality is indicated by A260/A280 and A260/A230 absorbance ratios. Expected values for pure RNA samples are  $\sim 2.0$  for A260/A280 and 2.0–2.2 for A260/A230 (51).

All extracted RNA samples had an A260/A280 value of approximately 2.0, satisfying the requirement. However, A260/A230 values were observed in a broader range. While most samples exhibited A260/A230 values in the range of 1.50–2.10, a few values were as low as 1.00, and even 0.40. All such samples exhibited a characteristic shoulder at  $\sim 230$  nm. A study by the extraction kit manufacturer states that low A260/A230 values "*almost always due to contamination with guanidine thiocyanate, a salt which absorbs very strongly at 220–230 nm and is present at very high concentrations in the lysis buffer or extraction reagent*" of most RNA extraction procedures. Further, the paper argues that guanidine thiocyanate concentrations "*up to 100 mM in an RNA sample do not compromise the reliability of real-time RT-PCR*". From the A260/A230 values we observed, the concentration of guanidine thiocyanate in our samples can be estimated to be up to a maximum of 1–2 mM (52). Therefore we conclude that even the lowest A260/A230 values seen in few single samples should not significantly affect our qPCR experiments.

### 4.3. Relative quantification of gene expression

#### 4.3.1. Amplification efficiency

In practice, when calculating PCR efficiencies, a result between 90 %–110 % is acceptable (44). These values translate to 1.9–2.1 in LinRegPCR calculation. The mean amplification efficiency of all valid samples was calculated to be  $1.931 \pm 0.063$ . A total of 16 samples where amplification was not detected, or was notably limited, were excluded from this calculation. These cases of inefficiency were mostly due to pipetting errors of the liquid handling system, which prevented the transfer of the complete PCR reaction mixture into the capillaries. We also calculated the amplification efficiencies calculated for each gene separately. These data are summarized in Table VIII.

Table VIII. Amplification efficiencies of target genes.

Gene	Mean efficiency	Standard deviation	# of valid samples
<i>Dusp6</i>	1.927	$\pm 0.027$	46 / 48
<i>Gng12</i>	1.931	$\pm 0.037$	47 / 48
<i>Ubqln2</i>	1.903	$\pm 0.020$	42 / 48
<i>Tifa</i>	1.917	$\pm 0.023$	48 / 48
<i>Gja1</i>	1.942	$\pm 0.037$	47 / 48
<i>Prkar2b</i>	2.003	$\pm 0.180$	47 / 48
<i>Bcl2</i>	1.930	$\pm 0.014$	45 / 48
<i>Ccl5</i>	1.917	$\pm 0.017$	48 / 48
<i>Adrb2</i>	1.923	$\pm 0.020$	48 / 48
<i>Slc7a11</i>	1.915	$\pm 0.016$	48 / 48

We have shown that the amplification efficiencies of most target genes, with the notable exception of *Prkar2b*, are comparable. The efficiencies are in the acceptable range of 90 %–110 %, and the observed standard deviations indicate a narrow data distribution. The standard deviation of the mean of all valid samples is  $\pm 3.3$  %. These findings underline the validity of the performed experiments and justify the choice of the  $\Delta\Delta C_T$  method for the calculation of relative gene expression.

In the case of *Prkar2b*, significant data scattering is seen, as indicated by the prominent standard deviation. The reason behind this occurrence could be unsuitable primers, or practical errors such as inaccurate pipetting of reaction components for this gene.

Amplification efficiencies of the reference genes *Gapdh* and *Actb* are calculated in Table IX. The efficiencies are in the desired interval, with the standard deviation indicating a narrow data distribution. The target genes and reference genes also appear to be amplified with comparable efficiency. Thereby we conclude that regarding amplification efficiency, both *Gapdh* and *Actb* are suitable for use as reference genes.

Table IX. Amplification efficiencies of reference genes *Gapdh* and *Actb*.

<b>Reference gene</b>	<b>Mean efficiency</b>	<b>Standard deviation</b>	<b># of valid samples</b>
<i>Gapdh</i>	1.904	± 0.020	47/48
<i>Actb</i>	1.960	± 0.028	47/48

### 4.3.2. Relative quantification

From the obtained qPCR data, we calculated relative expression ratios of the test samples (DRAW cells, and RAW264.7 cells newly infected with either DA or GDVII virus) compared to the control sample (RAW264.7 cells).

The relative expression ratio of the target genes in persistently infected DRAW cells compared to the control RAW264.7 cells is presented in Figure 12.

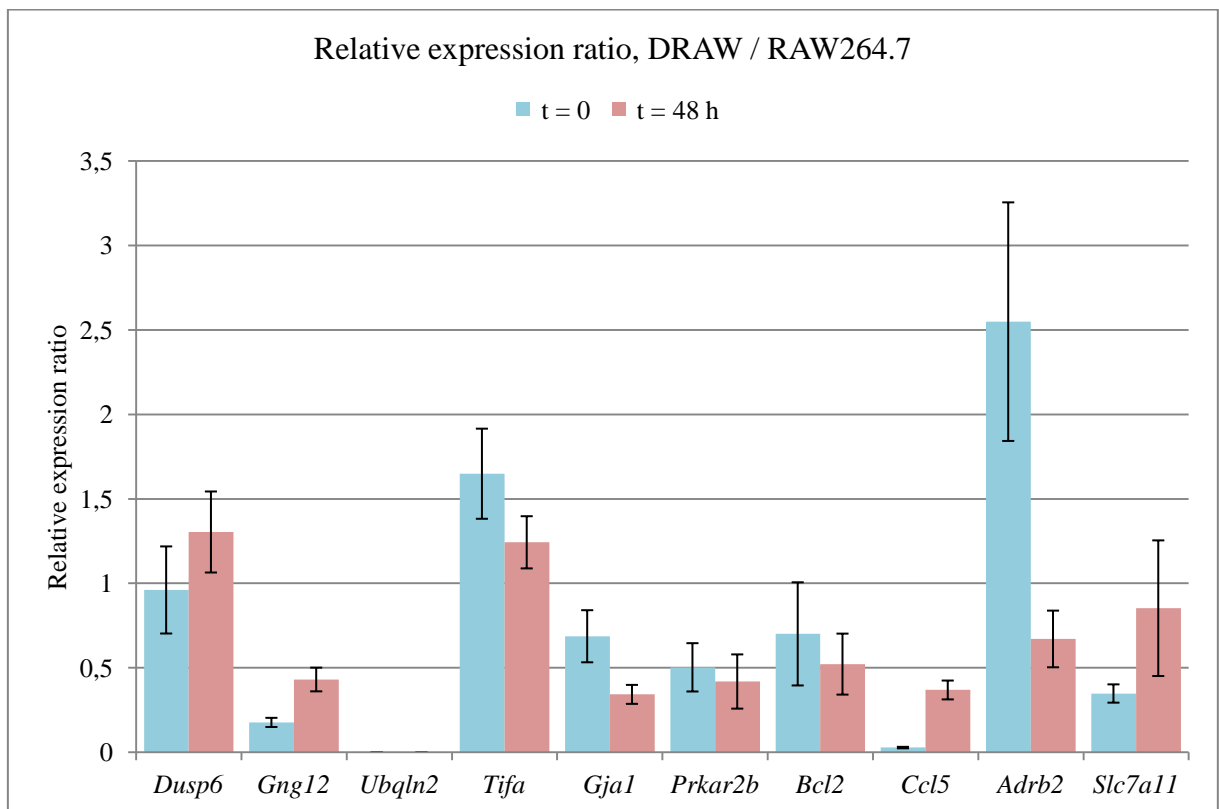


Figure 12. Relative expression ratios for DRAW / RAW264.7. All data are presented as the mean  $\pm$  SD.

The relative expression determined by qPCR was then compared to the relative expression previously determined by whole-genome DNA microarray at the host department (unpublished). The findings are collected in Table X. These findings are further examined in § 5. (Discussion).

Table X. Target gene expression ratios in DRAW cells compared to control RAW264.7 cells, as determined by qPCR and DNA microarray.

<b>Gene</b>	<b>qPCR expression</b>	<b>DNA microarray expression</b>	<b>Validated</b>
<i>Dusp6</i>	Unaffected at t = 0 h Unaffected at t = 48 h	Unaffected at t = 0h Unaffected at t = 48 h	Yes
<i>Gng12</i>	Downregulated at t = 0 h Downregulated at t = 48 h	Unaffected at t = 0h Downregulated at t = 48 h	No
<i>Ubqln2</i>	Downregulated at t = 0 h Missing data at t = 48 h	Downregulated at t = 0 h Downregulated at t = 48 h	No
<i>Tifa</i>	Upregulated at t = 0 h Unaffected at t = 48 h	Upregulated at t = 0h Unaffected at t = 48 h	Yes
<i>Gja1</i>	Downregulated at t = 0 h Downregulated at t = 48 h	Downregulated at t = 0 h Downregulated at t = 48 h	Yes
<i>Prkar2b</i>	Downregulated at t = 0 h Downregulated at t = 48 h	Downregulated at t = 0 h Unaffected at t = 48 h	No
<i>Bcl2</i>	Unaffected at t = 0 h Downregulated at t = 48 h	Unaffected at t = 0 h Unaffected at t = 48 h	No
<i>Ccl5</i>	Downregulated at t = 0 h Downregulated at t = 48 h	Downregulated at t = 0h Unaffected at t = 48 h	No
<i>Adrb2</i>	Upregulated at t = 0 h Unaffected at t = 48 h	Upregulated at t = 0 h Unaffected at t = 48 h	Yes
<i>Slc7a11</i>	Downregulated at t = 0 h Unaffected at t = 48 h	Unaffected at t = 0h Unaffected at t = 48 h	No

Further, we have compared relative expression ratios of the target genes for the newly infected RAW264.7 cells, (RAW264.7 + DA) and (RAW264.7 + GDVII), to the control sample (RAW264.7). The results are presented in Figure 13.

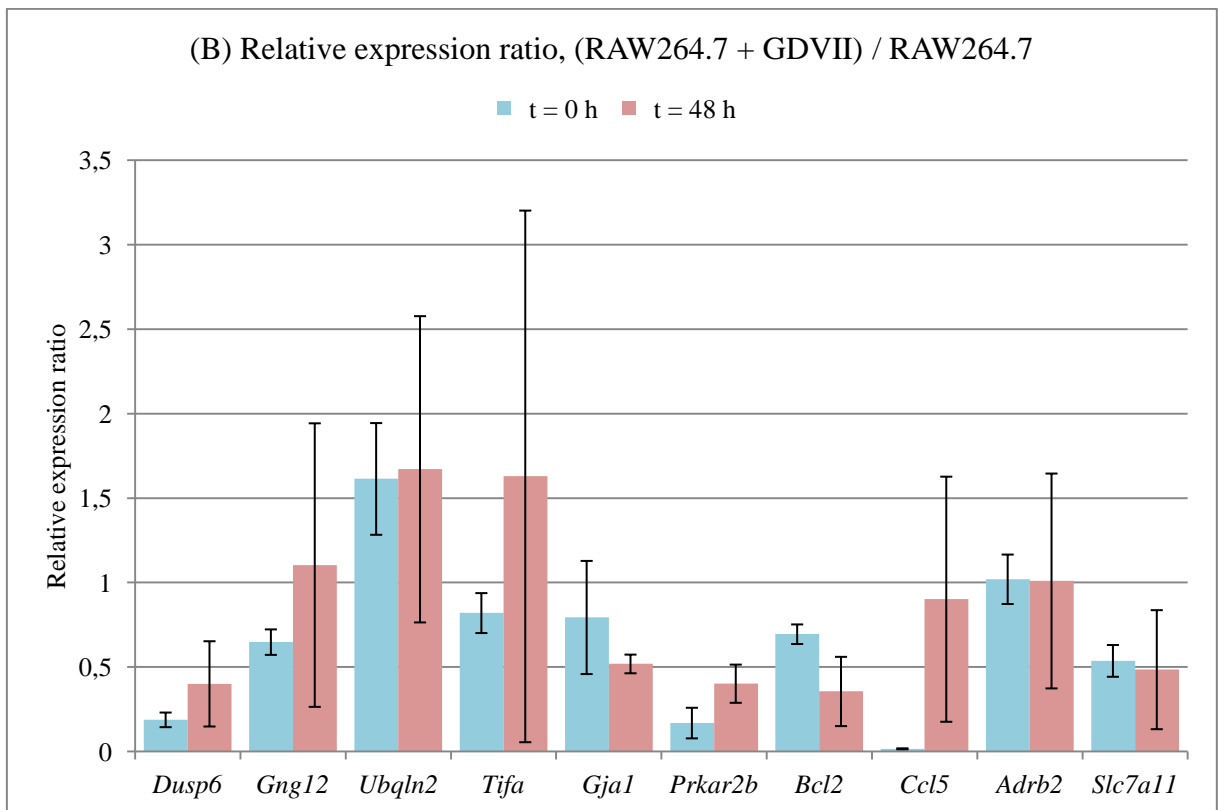
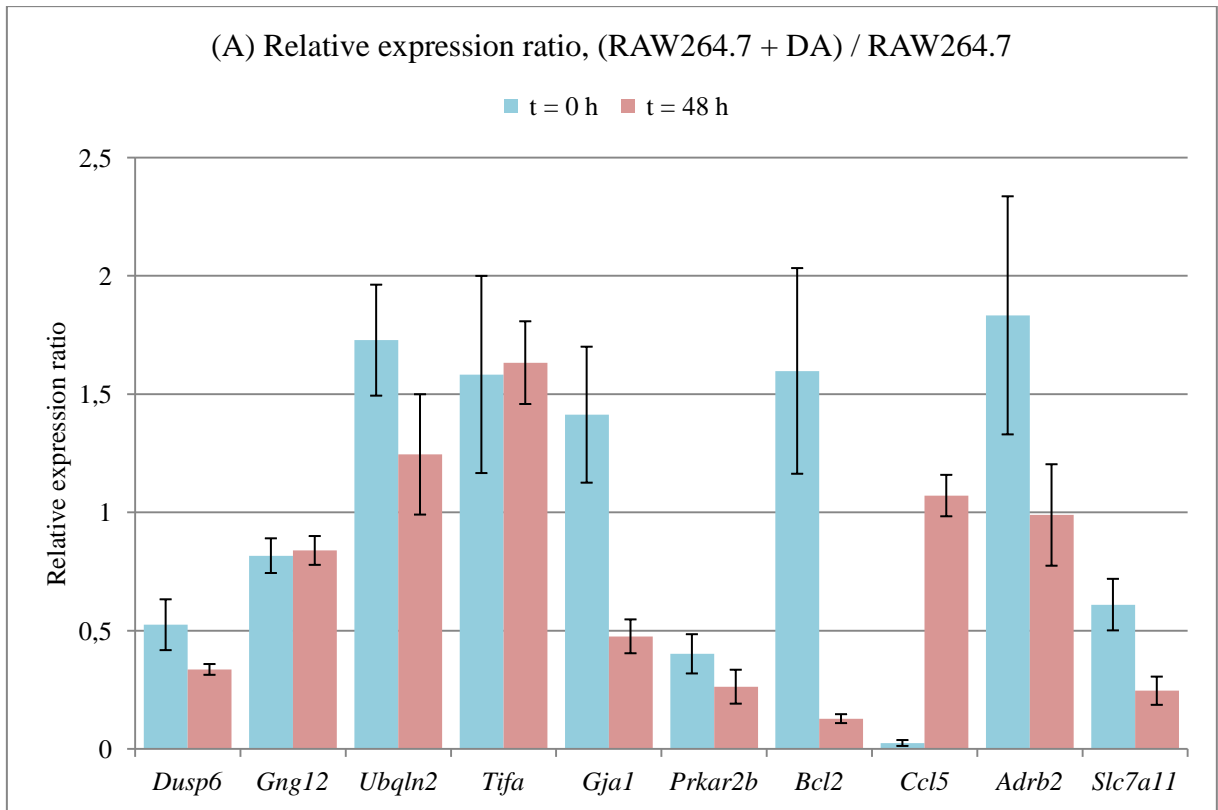


Figure 13. Relative expression ratios of target genes in RAW264.7 cells, newly infected with the DA (A) or GDVII (B) strain of TMEV, compared to the control sample (RAW264.7). All data are presented as the mean  $\pm$  SD.

Table XI. Target gene expression ratios in RAW264.7 macrophages, newly infected with the DA or GDVII strain of TMEV, compared to control RAW264.7 cells.

<b>Gene</b>	<b>DA infection</b>	<b>GDVII infection</b>
<i>Dusp6</i>	Downregulated at t = 0 h Downregulated at t = 48 h	Downregulated at t = 0 h Downregulated at t = 48 h
<i>Gng12</i>	Unaffected at t = 0 h Unaffected at t = 48 h	Downregulated at t = 0h Unaffected at t = 48 h
<i>Ubqln2</i>	Upregulated at t = 0 h Unaffected at t = 48 h	Upregulated at t = 0 h Upregulated at t = 48 h
<i>Tifa</i>	Upregulated at t = 0 h Upregulated at t = 48 h	Unaffected at t = 0 h Upregulated at t = 48 h
<i>Gja1</i>	Upregulated at t = 0 h Downregulated at t = 48 h	Unaffected at t = 0 h Downregulated at t = 48 h
<i>Prkar2b</i>	Downregulated at t = 0 h Downregulated at t = 48 h	Downregulated at t = 0 h Downregulated at t = 48 h
<i>Bcl2</i>	Unaffected at t = 0 h Downregulated at t = 48 h	Unaffected at t = 0 h Downregulated at t = 48 h
<i>Ccl5</i>	Downregulated at t = 0h Unaffected at t = 48 h	Downregulated at t = 0h Unaffected at t = 48 h
<i>Adrb2</i>	Upregulated at t = 0 h Unaffected at t = 48 h	Unaffected at t = 0 h Unaffected at t = 48 h
<i>Slc7a11</i>	Downregulated at t = 0 h Downregulated at t = 48 h	Downregulated at t = 0 h Downregulated at t = 48 h

### 4.3.3. Melting curve analysis

Melting curves of all samples were visually examined. We observed well-defined single peaks of the specific target amplicons in all samples. This confirms the absence of primer dimers and other non-specific amplification products. An example of representative melting curves is shown in Figure 14.

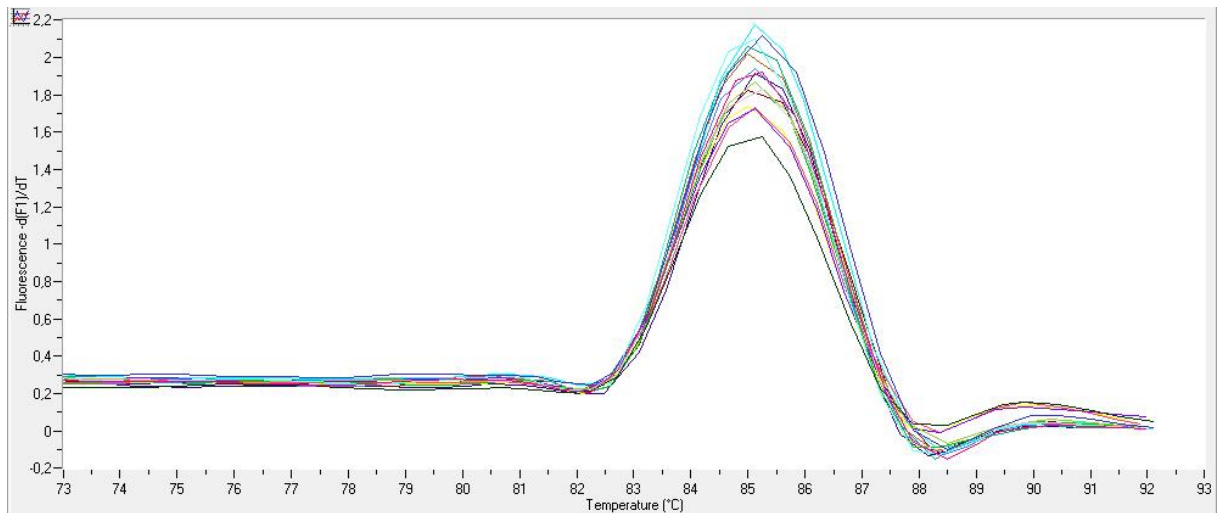


Figure 14. Melting curves obtained in the analysis of 16 *Gng12* samples.

Only in a single case, with one of the *Ubqln2* samples, we noticed an additional peak in the melting curve. It is unlikely that it represents primer dimer amplification, since dimers would likely also appear in other samples employing the same primer set. Presumably, the additional peak is a result of random nucleic acid contamination, such as genomic DNA contamination during sample and reagent handling.

## 5. DISCUSSION

### 5.1. Target gene expression

By analyzing the relative expression of target genes in our samples, we were able to elaborate on their involvement in the mechanisms of viral persistence, and other associated processes and pathways. Here, we touch upon the physiological role of each target gene and its protein transcript, investigate its role in demyelinating disease, and address the significance of the gene expression results we have observed in our experiments.

#### 5.1.1. *Dusp6*

*Dusp6* is a gene encoding the protein dual specificity phosphatase 6 (DUSP6). The substrate of this intracellular enzyme is extracellular signal-regulated kinase 1/2 (ERK1/2), a kinase from the mitogen-activated protein kinase (MAPK) family. MAPKs are a family of serine/threonine-specific protein kinases that play a role in cellular signaling, specifically at the end of the MAPK cascade. This phosphorylation cascade is initiated by ligand binding to a receptor tyrosine kinase (RTK), which results in the multiplication of the initial signal by several orders of magnitude. The ensuing phosphorylation of nuclear transcription factors results in gene transcription (40). DUSP6 catalyzes the dephosphorylation of threonine and tyrosine residues on ERK1/2, thereby inactivating the kinase.

Domercq *et al.* recently identified *Dusp6* as upregulated in oligodendroglial cultures stimulated with 2-amino-3-(3-hydroxy-5-methyl-isoxazol-4-yl)propanoic acid (AMPA) to induce apoptosis, in rat optic nerves treated with glutamate, as well as in optic nerves from MS patients before the appearance of damage to oligodendrocytes and axons. The research team also confirmed the necessity of *Dusp6* expression for oligodendrocyte death via glutamate excitotoxicity, a mechanism which has been implicated in the pathology of MS (KK). A similar pattern to the oligodendrocyte damage in MS is also seen in persistent TMEV infection, where oligodendrocytes are one of the sites of viral persistence (8). Oligodendrocyte death and the subsequent demyelination in TMEV infection may be caused by apoptosis, or by direct lytic infection (53).

In our qPCR experiments, as well as in the DNA microarray experiments, we identified *Dusp6* expression as unaffected at t = 0 h and t = 48 h. Upregulation at t = 48 h was present in both experiments, but not statistically significant. Nonetheless, this observation may indicate a degree of *Dusp6* involvement in persistent TMEV infection. In RAW264.7 cells newly infected with either the DA or GDVII strain of TMEV, *Dusp6* was significantly downregulated at both sampling times.

To our best knowledge, expression of *Dusp6* in macrophages has not been previously evaluated in the context of demyelination. Given its upregulation in oligodendrocytes in MS, it may also be involved in the pathology of persistent infection with TMEV, although not necessarily in infected macrophages. *Dusp6* expression analysis in TMEV infection *in vivo* may be needed to provide additional information on the subject.

The downregulation of *Dusp6* we observe in newly infected RAW264.7 cells may be related to a possible restriction of macrophage apoptosis in persistent TMEV infection, which we further address in § 5.1.5.

### **5.1.2. *Gng12***

*Gng12* is a gene encoding the gamma 12 subunit of G protein (GNG12), a heterotrimeric membrane protein involved in signal transduction. G proteins are the components of G protein-coupled receptors (GPCRs) that activate an effector enzyme in response to a signal (40). Amongst many other functions, several pathways exist by which GPCRs can signal to MAPKs, specifically ERK1/2 (54).

Larson *et al.* described the involvement of *Gng12* in the negative regulation of inflammation, where it might represent an important signaling component of the inflammatory cascade. *Gng12* was upregulated in BV-2, a murine microglial cell line, after lipopolysaccharide-induced inflammation. This was validated in experiments using primary microglia (55). Activated microglia are also found in areas featuring demyelinating lesions in MS patients (24), where they may play a role in the early stages of demyelination. They are also one of the inflammatory cell types in persistent TMEV infection (8). Therefore, given the high conservation of *Gng12* homologs, the gene could be of importance in MS-related inflammation, one of the hallmarks of MS pathology.

Using qPCR, we found *Gng12* to be significantly downregulated in DRAW cells at both sampling times. In the DNA microarray results, however, the downregulation at t = 0 h was not statistically significant. In the newly infected RAW264.7 cells, no statistically significant changes in *Gng12* expression were observed, despite lowered expression levels in DA infection, and at t = 0 h p.i. in GDVII infection.

The *Gng12* downregulation we observed in TMEV-infected cells may be unrelated to inflammation, or it may influence the inflammatory response in a way that allows or disallows viral persistence. More insight into *Gng12*-related pathways in TMEV infection would be required to further comment on this topic.

### ***5.1.3. The ubiquitin pathway: Ubqln2 and Tifa***

Ubiquitin is a small, highly conserved protein, part of the ubiquitin-proteasome system (UPS) involved in protein degradation. In an ATP-dependent pathway involving three separate ligases, E1–E3, ubiquitin is covalently linked to proteins to mark them for degradation by the 26S proteasome. This mechanism of proteolysis is important for the elimination of defective proteins as well as for the regulation of cellular processes (40). *Ubqln2* is a gene encoding ubiquilin 2 (UBQLN2), an ubiquitin-like protein. Within the processes described above, ubiquilin 2 associates with proteasomes as well as ubiquitin ligases, potentially serving as a link between the ubiquitination mechanism and the proteasome (56).

The UPS plays several important roles within cellular processes, among them modulation of the immune and inflammatory responses. Abnormalities in the UPS can lead to a variety of diseases, including inflammatory diseases as well as autoimmune diseases such as rheumatoid arthritis and psoriasis (57). This could indicate a role of the system, and possibly *Ubqln2*, in the pathology of MS as well.

Human UBQLN2 has been shown to bind the ATPase domain of stress 70 protein chaperone (STCH), a member of the 70 kDa heat shock protein (Hsp70)–like gene family. This binding occurs via a region that is highly conserved in Hsp70 proteins (58). The localization of Hsp70 and Hsp90 in TMEV–infected BHK-21 cells has recently been investigated by Mutsvunguma *et al.*, who suggested a possibility of an important, yet still unknown role of those proteins in viral folding and assembly (59).

*Ubqln2* was found to be significantly downregulated in DNA microarray experiments. However, with qPCR, we were unable to confirm this finding. We detected no amplification of *Ubqln2* in DRAW cells in 4 of the 12 samples, while another sample was missing completely. Further, in the statistical analysis of the remaining samples, a single *Ubqln2* sample in DRAW cells satisfied the inclusion criteria of the software. This prevented calculation of relative expression ratios for *Ubqln2* in DRAW cells. Since in the DNA microarray, *Ubqln2* in DRAW cells was expressed at much lower levels than any other target gene, the possibility exists that it was underexpressed strongly enough to not be detected by qPCR. However, since qPCR is a method with higher sensitivity than DNA microarrays, the validity of this reasoning is questionable. Conversely, *Ubqln2* was significantly upregulated in both newly infected RAW264.7 cells at all times, except at t = 48 h p.i. in DA infection.

The above considerations regarding a role of UBQLN2 in TMEV folding and assembly suggest a possible connection to TMEV persistence. However, due to missing data, we can not make a valid conclusion regarding the downregulation seen in DRAW cells, and this experiment needs to be repeated to exclude potential experimental mistakes. The upregulation of *Ubqln2* seen in the newly infected RAW264.7 cells may additionally indicate its involvement in viral persistence, and should be further considered and investigated.

*Tifa* is a gene encoding the protein TRAF-interacting protein with a forkhead-associated domain-containing protein A (TIFA). TIFA also plays a role in the ubiquitin pathway. As *Ea et al.* have shown, TIFA, while in an oligomerized form itself, induces the oligomerization and polyubiquitination of TRAF6, a protein from the TNF receptor-associated factor (TRAF) protein family. TRAF6 is an E3 ubiquitin ligase, yet its main function is not the targeting of protein degradation (60). Rather, in the interaction with E2 ligases, it possesses the ability to catalyze polyubiquitin chain formation (61), resulting in activation of downstream kinase cascades, important in inflammation and immunity. This pathway includes transforming growth factor  $\beta$ -activated kinase (TAK1) and I $\kappa$ B kinase (IKK), and their activation finally results in the regulation of gene expression by the protein complex NF- $\kappa$ B. This activation is mediated by the TIFA-induced oligomerization and polyubiquitination of TRAF6 (60).

*Tifa* was found to be significantly upregulated in DRAW cells at  $t = 0$  h and unaffected at  $t = 48$  h, by both qPCR and DNA microarrays. It was significantly upregulated at both sampling times in RAW264.7 cells newly infected with DA virus, while in GDVII infection, it was unaffected at  $t = 0$  h, and significantly upregulated at  $t = 48$  h p.i.

To our best knowledge, the role of *Tifa* in TMEV infection has so far not yet been investigated. The upregulation of *Tifa* we have observed at certain times in TMEV infection may indicate its involvement in the inflammatory or immune response to the virus. However, this is difficult to analyze based on the limited findings in an *in vitro* system, and additional investigations will likely be necessary.

#### 5.1.4. *Gjal*

*Gjal* is a gene encoding gap junction alpha-1 protein (GJA1), commonly known as connexin 43 (Cx43). Connexins are a family of membrane proteins that in vertebrates form gap junction channels. Gap junctions allow highly regulated direct communication between neighboring cells.

In CNS glia, gap junctions are found between oligodendrocytes, astrocytes, oligodendrocytes and astrocytes, and between myelin membrane layers in compact myelin. Cx43 is a connexin expressed in astrocytes, but not in oligodendrocytes. Although all aspects of gap junction communication in myelinating glia are not yet understood, it is clear that this coupling is vital for myelination and axonal survival (62). While oligodendrocyte connexin mutations can cause several human disorders that result in demyelination (63), the simultaneous loss of astrocyte connexins Cx43 and Cx30 was also shown to affect oligodendrocytes and myelin (64). However, the lack of astrocytic expression of both connexins was shown to not significantly influence the course of EAE (65).

Significant downregulation of *Gjal* was seen in DRAW macrophages in both qPCR and DNA microarray experiments. If this downregulation also occurs in astrocytes, another site of TMEV persistence (8), it may contribute to the demyelination that is seen in the persistent TMEV infection. The significance of this reasoning remains to be investigated.

Cx43 is also known to be expressed by macrophages, and constitutes the gap junctions between contacting macrophages. It is also implicated during inflammation, where it appears to be associated with macrophage and monocyte infiltration (66). The downregulation of *Gjal* may therefore affect macrophage behaviour in TMEV infection or even play a role in viral persistence.

In RAW264.7 cells, newly infected with DA virus, *Gjal* was significantly upregulated at  $t = 0$  h and significantly downregulated at  $t = 48$  h p.i., while in GDVII infection, it was unaffected at  $t = 0$  h and significantly downregulated at  $t = 48$  h p.i. These findings may represent a temporal shift in expression of a currently unknown importance.

### 5.1.5. Apoptosis: *Prkar2b* and *Bcl2*

The expression of *Bcl2* and *Prkar2b* is connected to apoptosis, the process of programmed cell death. In addition to roles in development, DNA damage and others, apoptosis can also occur in response to viral infection to prevent virus spread (40). Depending on the initiating signal, two distinct pathways of apoptosis exist: an intrinsic, mitochondrial apoptotic pathway initiated by cellular stress (including viral infection), and an extrinsic apoptotic pathway that involves ligand binding to death receptors (14,67).

As mentioned in § 1. (Introduction), apoptosis plays a role in persistent TMEV infection, as well as in MS. The process appears to be dependent on cellular permissiveness for the infection, leading to apoptosis in cells restrictive to viral replication, and cytopathic effects in permissive cells. Exactly which types of cells undergo apoptosis in TMEV infection is still not definitively established. Conflicting reports exist, with the different outcomes possibly dependent on experimental design or differences in viral strains (14). Apoptotic neurons of the grey matter are seen in the early acute phase of both DA and GDVII infection (10). In the late chronic phase *in vivo*, T lymphocytes, oligodendrocytes, and possibly astrocytes all may or may not undergo apoptosis. Microglia may be persistently infected with or without the presence of apoptosis (14).

Macrophages, bearing the main viral antigen burden in persistent TMEV infection *in vivo*, become infected and, to some degree, undergo apoptosis *in vitro* (14). Of most relevance to our model appear to be the findings of Ghadge *et al.* They show that the L\* protein, only expressed by strains of the persistent TO group, has an anti-apoptotic effect in persistent DA strain infection of macrophages *in vitro*. Thereby, it may also enable viral persistence (19). Considering this, DRAW cells, as persistently DA strain–infected macrophages, are a suitable model for studying the effect of TMEV infection on apoptosis.

Apoptosis also plays a role in MS. In this disease, several patterns of demyelination exist, one of which is associated with oligodendrocyte apoptosis, which may therefore represent a mechanism of tissue damage in MS. Further, as noted earlier, T lymphocytes in both MS and late phase DA infection may share a related impairment of the apoptotic pathway, related to *Bcl2* expression and possibly enabling demyelination (8).

*Prkar2b* is a gene encoding the protein PRKAR2B. This protein is the type II-beta regulatory subunit of protein kinase A (PKA), also known as cyclic adenosine monophosphate (cAMP)-dependent protein kinase, a tetramer of two regulatory and two catalytic subunits (68). When cAMP binds to the regulatory subunit of PKA, a conformational change releases the catalytic subunit, activating PKA. Activated PKA catalyzes the phosphorylation of other proteins, thereby regulating several enzymes with diverse functions (40).

PKA has a wide role throughout the organism. Relevant to our research, it is also involved in apoptosis. cAMP signaling to PKA, and the subsequent phosphorylation, has a pro-apoptotic effect by an intrinsic mechanism. The identity of the specific protein targets is currently unknown. Additionally, PKA can also have an anti-apoptotic effect by a different mechanism. Despite reports linking PKA I and II isozymes to apoptosis and cancer (69), no direct connection of *Prkar2b* to viral persistence or demyelinating disease has, to our knowledge, so far been found.

*Prkar2b* was significantly downregulated in DRAW cells in the qPCR experiments, and at  $t = 0$  h in the DNA microarray, however it was unaffected at  $t = 48$  h in the DNA microarray. This downregulation in DRAW cells may be related to the prevention of macrophage apoptosis as seen in persistent TMEV infection. Further investigation into the possibility of this PKA subunit as a target in demyelinating disease treatment would be required. *Prkar2b* was further significantly downregulated at both sampling times in RAW264.7 cells newly infected with either DA or GDVII virus, which may indicate inhibition of macrophage apoptosis in early acute disease. However, such an inhibition would need to be mediated by a mechanism other than the anti-apoptotic effect of the L\* protein, since L\* is not expressed in GDVII infection.

*Bcl2* is a gene encoding the protein B-cell lymphoma 2 (BCL-2), a member of the Bcl-2 protein family. Members of this family regulate the intrinsic apoptotic pathway with either pro- or anti-apoptotic activity. BCL-2 is an anti-apoptotic protein, blocking the apoptotic death of certain cells by binding pro-apoptotic proteins (67). It is typically found on the outer mitochondrial membrane and endoplasmic reticulum membrane (70).

Oleszak *et al.* have demonstrated the involvement of *Bcl2* expression in the infection with TMEV, DA strain. Specifically, *Bcl2* expression in CNS-infiltrating T cells is low in early acute infection, leading to apoptosis and resolution of inflammation. In the late chronic infection, very little apoptosis is seen, as T lymphocytes express *Bcl2*. This may lead to T cell accumulation in the CNS and play a role in demyelination (71). Regarding BCL-2 role in macrophages, RAW264.7 cells were transfected with human BCL-2 by Meßmer *et al.* The resulting cells were resistant to nitric oxide-induced apoptosis, suggesting an anti-apoptotic role of BCL-2 in these cells (72).

*Bcl2* expression in DRAW cells, as detected by qPCR, appears to be unaffected at  $t = 0$  h, while the gene is significantly downregulated at  $t = 48$  h. A similar pattern is seen in the cells newly infected with DA or GDVII virus. In the DNA microarray results for DRAW cells, expression is unaffected at both times. Given the apparent importance of macrophage apoptosis, or the limitation thereof, in TMEV infection, these results are unexpected, especially considering the aforementioned role of *Bcl2* in apoptosis.

#### 5.1.6. *Ccl5*

*Ccl5* is a gene encoding the protein chemokine (C-C motif) ligand 5 (CCL5), commonly known as "regulated on activation, normal T cell expressed and secreted" (RANTES). RANTES belongs to the family of cytokines, secreted proteins involved in the inflammatory and immune responses. As a chemotactic cytokine (chemokine), RANTES is a chemoattractant for blood monocytes, memory T helper cells and eosinophils. It also causes histamine release from basophils and activates eosinophils (73).

Cytokines, including chemokines, play an important role in the induction and regulation of the immune response to viral infections, and may be involved in their pathogenesis and persistent infections. In TMEV infection, relevant cytokines are produced by inflammatory infiltrates, as well as by CNS cells such as astrocytes or microglia (8). This pattern is also observed in MS, where infiltrating cells, astrocytes, and microglia also express various cytokines (24). RANTES was shown to be produced in MS by perivascular inflammatory

cells, and its levels in the cerebrospinal fluid of MS patients were significantly increased during symptomatic episodes of inflammatory demyelination (74).

Using qPCR, we found *Ccl5* to be significantly downregulated at both sampling times. This is unexpected, and in contrast with the findings in DNA microarrays, where *Ccl5* was downregulated at t = 0 h, and upregulated, but not significantly, at t = 48 h. In RAW264.7 cells newly infected with either DA or GDVII virus, *Ccl5* was significantly downregulated at t = 0 h, but not significantly affected at t = 48 h p.i.

Interestingly, a downregulation of *Ccl5* in TMEV infection is contrary to the findings of several other investigators, eg., Palma and Kim detected upregulation of RANTES in BeAn strain TMEV–infected cultures of oligodendrocytes, astrocytes and microglia (75). This includes Steurbaut *et al.*, who detected an upregulation of RANTES in DRAW cells with the use of a protein array (35). Therefore in our experiments, potential experimental mistakes cannot be excluded, especially since *Ccl5* expression as detected by qPCR and DNA microarray does not appear to correspond. However, the initial downregulation and subsequent normalization of *Ccl5* expression in newly infected RAW264.7 cells may be an indicator of TMEV involvement kinetics in the chemokine regulation of the antiviral immune response.

#### **5.1.7. *Adrb2***

The gene *Adrb2* encodes the adrenergic receptor beta 2 (ADRB2), a well-understood GPCR. This receptor initiates a signaling pathway in response to the binding of its ligands, adrenaline and noradrenaline (40).

Using qPCR, we have validated a temporally specific expression pattern of *Adrb2* which was also seen in DNA microarray experiments. The gene is significantly upregulated at t = 0 h, while at 48 h, expression is unaffected; downregulation at t = 48 h is seen in both cases, but it is not statistically significant. The gene is also significantly upregulated at t = 0 h in RAW264.7 cells newly infected with the DA virus, but not at t = 48 h p.i., where it is unaffected. Expression is also unaffected at both sampling points in GDVII infection.

The effect of noradrenaline and adrenaline on macrophages appears to be highly complex. Generally, stimulation of alpha-2 adrenergic receptors is stimulatory, while ADRB2 stimulation inhibits macrophages. Alpha adrenergic receptor expression and ADRB2 responsiveness depends on the state of macrophage activation, and on several factors in the cellular environment. Simultaneously, several additional mediators also influence macrophage activity (76). A variation in ADRB2 expression in macrophages may influence the extent of CNS damage in TMEV infection and MS, although this is difficult to assess in the relatively simplistic environment of a cell line such as DRAW.

The roles of ADRB2 in astrocytes have been extensively reviewed by Laureys *et al.* Activation of these receptors regulates an array of inflammatory and immune responses, exhibiting a dual, pro-inflammatory and neuroprotective role in astrocyte gene expression. A dysregulation of astrocytal ADRB2 has been implicated in the pathology of MS. A deficiency of this receptor is found in MS patients in MS plaques and normal appearing white matter, whereas astrocytal ADRB2 would normally be upregulated in areas of neuronal injury. The possibility of viral etiology of MS is additionally open, as similar observations were made in dogs presenting with canine distemper encephalitis, a disease and viral MS model caused by the canine distemper virus (CDV) (77). This observation further suggests the possibility of a similar pattern in TMEV infection.

To our best knowledge, no direct connection between TMEV infection and the expression of *Adrb2* has so far been established. Even though we have gained some insight into ADRB2 expression in DRAW and newly infected RAW264.7 cells, the use of an *in vivo* model, and observation over a longer period, would likely be required to provide better insight into the role of ADRB2 in TMEV infection.

Finally, we can draw at least two associations between *Adrb2* and some of our remaining target genes. First, ADRB2 is a GPCR, and one of the gamma subunits of the G protein it is coupled with may be GNG12 (78). Second, if the G protein associated with ADRB2 is the stimulatory G protein ( $G_s$ ), then ligand binding to ADRB2 stimulates the production of cAMP by adenylyl cyclase, and cAMP in turn activates PKA (40), of which PRKAR2B can be a regulatory subunit. Any significance those genes have in TMEV infection may be further studied in regard to an *Adrb2* connection as well.

### 5.1.8. *Slc7a11*

*Slc7a11* is a gene encoding the protein solute carrier family 7 (anionic amino acid transporter light chain,  $x_c^-$  system), member 11 (SLC7A11), also known as xCT. This protein is the catalytic subunit of the cystine/glutamate antiporter  $x_c^-$ , a heterodimeric anionic amino acid transport system (79). The main function of this system is to provide cystine for the synthesis of the antioxidant glutathione (80).

Glutamate excitotoxicity has been implicated in the pathology of MS, specifically in demyelination. Monocytes release glutamate through the  $x_c^-$  system, and activation of monocytes results in an upregulation of the xCT subunit, resulting in increased glutamate release. xCT was shown to be upregulated in activated macrophages and microglia in both EAE and MS. These findings propose the  $x_c^-$  system as a link between inflammatory response, specifically the monocyte-macrophage-microglia lineage, and glutamate excitotoxicity in demyelinating disease (80).

Considering the above implications, the results seen in our experiments are contrary to our expectations. In DRAW macrophages, *Slc7a11* was found to be significantly downregulated at  $t = 0$  h and unaffected at  $t = 48$  h in the qPCR experiments. However, it was unaffected at both these times in the DNA microarray results. The gene was also downregulated at both sampling times in the RAW264.7 cells newly infected with DA or GDVII virus. Possibly, the complexity of an *in vivo* system is required to observe the aforementioned mechanisms in the context of a demyelinating disorder.

## 5.2. Conclusion

The aim of this thesis was to use RT real-time qPCR to validate the expression of 10 target genes in DRAW cells as previously determined by DNA microarrays. We have successfully validated the expression of four out of 10 target genes at both sampling times (t = 0 h and t = 48 h): *Dusp6*, *Tifa*, *Gjal*, and *Adrb2*.

New test DRAW and control RAW264.7 cells have been cultivated for the use in qPCR experiments. Therefore, the confirmation of gene expression that we observed in these new sample cells is stronger than a confirmation that would be observed in the same sample cells already used in the DNA microarray experiments.

We were unable to validate the DNA microarray results of gene expression for four genes: *Prkar2b*, *Bcl2*, *Ccl5* and *Slc7a11*. In one gene, *Gng12*, a very similar pattern of expression to the DNA microarray results was seen with qPCR, however the statistical significance of the findings differed. In each of these five cases, we were able to validate the results at one of the sampling points (t = 0 h and t = 48 h), but not at the other. Further, at all points where expression was not validated, there was never a completely opposite result in expression (upregulation in one case, downregulation in the other) seen with the two research methods.

Several reasons may exist why validation was not achieved in these cases. First, the expression of those genes may not be involved enough in persistent TMEV infection to consistently be up- or downregulated at the sampling times. Second, the observed gene expression may differ between the DNA microarray and qPCR results due to the better sensitivity of the qPCR method, and therefore the obtained qPCR results may not necessarily be "false", even in the absence of DNA microarray result validation. However, additional experiments would be needed to confirm this. And third, experimental mistakes, or a suboptimal experiment design, unfortunately cannot be excluded completely.

Additionally, it should be noted that we were unable to comment on the expression of *Ubqln2* in DRAW due to insufficient data.

Regardless of whether validation of gene expression was seen or not, we attempted to obtain a wider perspective of the target gene functions in pathways related to TMEV infection, viral persistence, MS, and demyelinating disease in general. We studied previously published research on the role of these genes in such circumstances, particularly their expression in macrophages, where available. We then compared our findings to the previously published observations, and have suggested possible mechanisms and pathways in which the products of target genes could be involved in TMEV infection or persistence. We have also identified potential fields of further study involving those mechanisms and pathways, which are, for the most part, highly complex and diversely regulated. Additional studies will need to be performed to further elaborate these mechanisms, and the roles of the particular genes and their products within them.

Some of the gene expression results in DRAW cells, either validating the DNA microarray results or not, are unexpected considering the previously described roles of those genes. Several possible reasons for this exist. Notably, in DRAW cells, we observe virus-induced changes in gene expression in the relatively simplistic environment of a cell line, whereas in many of the previously published studies, gene expression was examined in the complexity of an *in vivo* system. Additionally, the observed expression may reflect changes to virus or host cells in persistent infection over time, as a consequence of co-evolution, which cannot be excluded.

We also analyzed the expression of target genes in RAW264.7 cells, newly infected with either the DA or GDVII strain of TMEV. The expression at  $t = 0$  h and  $t = 48$  h p.i. mostly corresponds between the two strains, and some of the findings may present a general response to viral presence or infection. Any differences in the findings, however, may indicate a gene that plays a role in the development of viral persistence, and would need to be investigated further.

We have investigated the expression of genes that were of interest to the host department. In the DNA microarray experiments, the expression of many additional genes was affected in DRAW cells as compared to RAW264.7 cells. Those findings should also be taken into consideration together with our results. Thereby, additional conclusions related to relevant pathways could be extrapolated to make further hypotheses regarding the mechanisms of persistent infection and demyelination.

To conclude, we believe that the DRAW cell line can be used as a valuable model for viral persistence and MS. Potentially, novel MS treatments that interfere with the role of macrophages in the disease can be preliminarily tested using this *in vitro* model.

## REFERENCES

1. King AMQ, Adams MJ, Carstens EB, Lefkowitz EJ (editors): Virus taxonomy: classification and nomenclature of viruses: Ninth Report of the International Committee on Taxonomy of Viruses, Elsevier Academic Press, San Diego, 2012, 835–9, 862–3.
2. Mahy BWJ, van Regenmortel MH (editors): Encyclopedia of virology, 3rd ed., Academic Press, Amsterdam, 2008: 1:440–8, 3:81–3, 5:37–45.
3. Brahic M, Bureau J-F, Michiels T: The genetics of the persistent infection and demyelinating disease caused by Theiler's virus. *Annu Rev Microbiol* 2005; 59: 279–98.
4. Lipton HL, Kim BS, Yahikozawa H, Nadler CF: Serological evidence that *Mus musculus* is the natural host of Theiler's murine encephalomyelitis virus. *Virus Res* 2001; 76: 79–86.
5. Theiler M: Spontaneous encephalomyelitis of mice, a new virus disease. *J Exp Med* 1937; 65: 705–19.
6. Lipton HL: Persistent Theiler's Murine Encephalomyelitis Virus Infection in Mice depends on Plaque Size. *J Gen Virol* 1980; 46: 169–77.
7. Lorch Y, Friedmann A, Lipton HL, Kotler M: Theiler's murine encephalomyelitis virus group includes two distinct genetic subgroups that differ pathologically and biologically. *J Virol* 1981; 40: 560–7.
8. Oleszak EL, Chang JR, Friedman H, Katsetos CD, Platsoucas CD: Theiler's virus infection: a model for multiple sclerosis. *Clin Microbiol Rev* 2004; 17: 174–207.
9. Theiler M: Encephalomyelitis of mice: I. Characteristics and pathogenesis of the virus. *J Exp Med* 1940; 72: 49–67.
10. Tsunoda I, Fujinami RS: Neuropathogenesis of Theiler's murine encephalomyelitis virus infection, an animal model for multiple sclerosis. *J Neuroimmune Pharmacol* 2009; 5: 355–69.
11. Aubert C, Brahic M: Early infection of the central nervous system by the GDVII and DA strains of Theiler's virus. *J Virol* 1995; 69: 3197–200.
12. Daniels JB, Pappenheimer AM, Richardson S: Observations on encephalomyelitis of mice (DA strain). *J Exp Med* 1952; 96: 517–30.

13. Lipton HL: Theiler's virus infection in mice: an unusual biphasic disease process leading to demyelination. *Infect Immun* 1975; 11: 1147–55.
14. Lavi E, Constantinescu CS: *Experimental models of multiple sclerosis*, Springer, New York, 2005, 579–709.
15. Lipton HL, Kumar ASM, Trottier M: Theiler's virus persistence in the central nervous system of mice is associated with continuous viral replication and a difference in outcome of infection of infiltrating macrophages versus oligodendrocytes. *Virus Res* 2005; 111: 214–23.
16. van Pesch V, van Eyll O, Michiels T: The leader protein of Theiler's virus inhibits immediate–early alpha/beta interferon production. *J Virol* 2001; 75: 7811–7.
17. Delhaye S, Van Pesch V, Michiels T: The leader protein of Theiler's virus interferes with nucleocytoplasmic trafficking of cellular proteins. *J Virol* 2004; 78: 4357–62.
18. Lipton HL, Twaddle G, Jelachich ML: The predominant virus antigen burden is present in macrophages in Theiler's murine encephalomyelitis virus–induced demyelinating disease. *J Virol* 1995; 69: 2525–33.
19. Ghadge GD, Ma L, Sato S, Kim J, Roos RP: A protein critical for a Theiler's virus–induced immune system–mediated demyelinating disease has a cell type–specific antiapoptotic effect and a key role in virus persistence. *J Virol* 1998; 72: 8605–12.
20. Roussarie J-P, Ruffié C, Brahic M: The role of myelin in Theiler's virus persistence in the central nervous system. *PLoS Pathog* 2007; 3: e23.
21. Bihl F, Pena-Rossi C, Guénet JL, Brahic M, Bureau JF: The shiverer mutation affects the persistence of Theiler's virus in the central nervous system. *J Virol* 1997; 71: 5025–30.
22. Compston A, Coles A: Multiple sclerosis. *Lancet* 2008; 372: 1502–17.
23. Chandrasoma P, Taylor CR: *Concise pathology*, 3rd Ed., Appleton & Lange, Stamford, 1998.
24. Cook SD (editor): *Handbook of multiple sclerosis*, 4th Ed., Taylor & Francis, New York, 2006.
25. <http://en.wikipedia.org/wiki/File:Nerve.nida.jpg>, Wikipedia image in public domain. Retrieved 3. 3. 2013.

26. Mecha M, Carrillo-Salinas FJ, Mestre L, Feliú A, Guaza C: Viral models of multiple sclerosis: Neurodegeneration and demyelination in mice infected with Theiler's virus. *Prog Neurobiol* 2013; 101–102: 46–64.
27. Kipp M, van der Star B, Vogel DYS, Puentes F, van der Valk P, Baker D, Amor S: Experimental in vivo and in vitro models of multiple sclerosis: EAE and beyond. *Mult Scler Relat Disord* 2012; 1: 5–28.
28. Chang JR, Zaczynska E, Katsetos CD, Platsoucas CD, Oleszak EL: Differential expression of TGF- $\beta$ , IL-2, and other cytokines in the CNS of Theiler's murine encephalomyelitis virus-infected susceptible and resistant strains of mice. *Virology* 2000; 278: 346–60.
29. Steurbaut S, Rombaut B, Vrijssen R: Persistent infection of RAW264.7 macrophages with the DA strain of Theiler's murine encephalomyelitis virus: An in vitro model to study viral persistence. *J Neurovirol* 2006; 12: 108–15.
30. Rossi CP, Delcroix M, Huitinga I, McAllister A, Van Rooijen N, Claassen E, Brahic M: Role of Macrophages during Theiler's Virus Infection. *J Virol* 1997; 71: 3336–40.
31. Pope JG, Vanderlugt CL, Rahbe SM, Lipton HL, Miller SD: Characterization of and functional antigen presentation by central nervous system mononuclear cells from mice infected with Theiler's murine encephalomyelitis virus. *J Virol* 1998; 72: 7762–71.
32. Katz-Levy Y, Neville KL, Padilla J, Rahbe S, Begolka WS, Girvin AM, Olson JK, Vanderlugt CL, Miller SD: Temporal development of autoreactive Th1 responses and endogenous presentation of self myelin epitopes by central nervous system-resident APCs in Theiler's virus-infected mice. *J Immunol* 2000; 165: 5304–14.
33. Himeda T, Okuwa T, Muraki Y, Ohara Y: Cytokine/chemokine profile in J774 macrophage cells persistently infected with DA strain of Theiler's murine encephalomyelitis virus (TMEV). *J Neurovirol* 2010; 16: 219–29.
34. Raschke WC, Baird S, Ralph P, Nakoinz I: Functional macrophage cell lines transformed by Abelson leukemia virus. *Cell* 1978; 15: 261–267.
35. Steurbaut S, Merckx E, Rombaut B, Vrijssen R: Modulation of viral replication in macrophages persistently infected with the DA strain of Theiler's murine encephalomyelitis virus. *Virol J* 2008; 5: 89.

36. Freshney RI: Culture of animal cells: a manual of basic technique and specialized applications, 6th ed., Wiley-Blackwell, Hoboken, 2010: 13, 109–11.
37. Qiagen FAQ: 101 - Why do I have to add beta-mercaptoethanol (beta-ME) to lysis Buffer RLT of the RNeasy Kits? <http://www.qiagen.com/Knowledge-and-Support/FAQ/?ID=eac3139e-6c6c-4172-b61f-18d61b6cdd1e>, retrieved 23. 2. 2013.
38. CellTiter-Blue Cell Viability Assay: Instructions for use of products G8080, G8081 and G8082. Promega Corporation part #TB317, revised 6/09.
39. McPherson M, Møller S: PCR the Basics, Taylor & Francis Ltd., Hoboken, 2006.
40. Nelson DL, Cox MM (editors): Lehninger principles of biochemistry, 5th ed., W.H. Freeman, New York, 2008.
41. Saiki RK, Scharf S, Faloona F, Mullis KB, Horn GT, Erlich HA, Arnheim N: Enzymatic amplification of beta-globin genomic sequences and restriction site analysis for diagnosis of sickle cell anemia. *Science* 1985; 230: 1350–4.
42. VanGuilder HD, Vrana KE, Freeman WM: Twenty-five years of quantitative PCR for gene expression analysis. *Biotechniques* 2008; 44: 619–26.
43. Pfaffl MW: Quantification strategies in real-time PCR. In: Bustin SA (editor): A–Z of quantitative PCR, International University Line, La Jolla, 2004, 87–112.
44. Eurogentec qPCR guide. <http://www.eurogentec.com/uploads/qPCR-guide.pdf>, retrieved 25. 2. 2013.
45. LightCycler FastStart DNA Master SYBR Green I. Roche, manual version October 2009.
46. Domercq M, Alberdi E, Sanchez-Gomez MV, Ariz U, Perez-Samartin A, Matute C: Dual-specific phosphatase-6 (Dusp6) and ERK mediate AMPA receptor–induced oligodendrocyte death. *J Biol Chem* 2011; 286: 11825–36.
47. Ramakers C, Ruijter JM, Deprez RHL, Moorman AF: Assumption-free analysis of quantitative real-time polymerase chain reaction (PCR) data. *Neurosci Lett* 2003; 339: 62–6.
48. Hellemans J, Mortier G, De Paepe A, Speleman F, Vandesompele J: qBase relative quantification framework and software for management and automated analysis of real-time quantitative PCR data. *Genome Biol* 2007; 8: R19.
49. McDonald, JH: Handbook of Biological Statistics, 2nd ed., Sparky House Publishing, Baltimore, Maryland, 2009: 123–126.

50. <http://people.richland.edu/james/lecture/m170/ch13-1wy.html>, retrieved 17. 3. 2013.
51. Thermo Scientific T042-Technical Bulletin, NanoDrop Spectrophotometers. <http://www.nanodrop.com/Library/T042-NanoDrop-Spectrophotometers-Nucleic-Acid-Purity-Ratios.pdf>, retrieved 5. 3. 2013.
52. von Ahlfen S, Schlumpberger M: Effects of low  $A_{260}/A_{230}$  ratios in RNA preparations on downstream applications. In: QIAGEN Gene Expression Newsletter 2010, Issue 15/10: 7–8. [http://b2b.qiagen.com/literature/gexnews/pdf/1061749\\_nlgef\\_issu15\\_310\\_lr.pdf](http://b2b.qiagen.com/literature/gexnews/pdf/1061749_nlgef_issu15_310_lr.pdf), retrieved 15. 3. 2013.
53. Sato F, Tanaka H, Hasanovic F, Tsunoda I: Theiler's virus infection: Pathophysiology of demyelination and neurodegeneration. *Pathophysiology* 2011; 18: 31–41.
54. [http://www.cellsignal.com/reference/pathway/MAPK\\_G\\_Protein.html](http://www.cellsignal.com/reference/pathway/MAPK_G_Protein.html), retrieved 8. 3. 2013.
55. Larson KC, Draper MP, Lipko M, Dabrowski M: Gng12 is a novel negative regulator of LPS-induced inflammation in the microglial cell line BV-2. *Inflamm Res* 2009; 59: 15–22.
56. <http://www.ncbi.nlm.nih.gov/gene/29978>, retrieved 8. 3. 2013.
57. Wang J, Maldonado MA: The ubiquitin-proteasome system and its role in inflammatory and autoimmune diseases. *Cell Mol Immunol* 2006; 3: 255–61.
58. Kaye FJ, Modi S, Ivanovska I, Koonin EV, Thress K, Kubo A, Kornbluth S, Rose MD: A family of ubiquitin-like proteins binds the ATPase domain of Hsp70-like Stch. *FEBS Lett* 2000; 467: 348–55.
59. Mutsvunguma LZ, Moetlhoa B, Edkins AL, Luke GA, Blatch GL, Knox C: Theiler's murine encephalomyelitis virus infection induces a redistribution of heat shock proteins 70 and 90 in BHK-21 cells, and is inhibited by novobiocin and geldanamycin. *Cell Stress Chaperones* 2011; 16: 505–15.
60. Ea C-K, Sun L, Inoue J-I, Chen ZJ: TIFA activates I B kinase (IKK) by promoting oligomerization and ubiquitination of TRAF6. *Proc Natl Acad Sci USA* 2004; 101: 15318–23.
61. <http://www.ncbi.nlm.nih.gov/gene/7189>, retrieved 13. 3. 2013.

62. Nualart-Marti A, Solsona C, Fields RD: Gap junction communication in myelinating glia. *BBA. Biomembranes* 2013; 1828: 69–78.
63. Cotrina ML, Nedergaard M: Brain connexins in demyelinating diseases: Therapeutic potential of glial targets. *Brain Res* 2012; 1487: 61–8.
64. Lutz SE, Zhao Y, Gulinello M, Lee SC, Raine CS, Brosnan CF: Deletion of astrocyte connexins 43 and 30 leads to a dysmyelinating phenotype and hippocampal CA1 vacuolation. *J Neurosci* 2009; 29: 7743–52.
65. Lutz SE, Raine CS, Brosnan CF: Loss of astrocyte connexins 43 and 30 does not significantly alter susceptibility or severity of acute experimental autoimmune encephalomyelitis in mice. *J Neuroimmunol* 2012; 245: 8–14.
66. Oviedo-Orta E, Howard Evans W: Gap junctions and connexin-mediated communication in the immune system. *BBA. Biomembranes* 2004; 1662: 102–12.
67. Brunelle JK, Letai A: Control of mitochondrial apoptosis by the Bcl-2 family. *J Cell Sci* 2009; 122: 437–41.
68. <http://www.ncbi.nlm.nih.gov/gene/5577>, retrieved 11. 3. 2013.
69. Insel PA, Zhang L, Murray F, Yokouchi H, Zambon AC: Cyclic AMP is both a pro-apoptotic and anti-apoptotic second messenger. *Acta Physiol (Oxf)* 2012; 204: 277–87.
70. <http://genatlas.medecine.univ-paris5.fr/fiche.php?symbol=bcl2>, retrieved 12. 3. 2013.
71. Oleszak EL, Hoffman BE, Chang JR, Zaczynska E, Gaughan J, Katsetos CD, Platsoucas CD, Harvey N: Apoptosis of infiltrating T cells in the central nervous system of mice infected with Theiler's murine encephalomyelitis virus. *Virology* 2003; 315: 110–23.
72. Meßmer UK, Reed JC, Brüne B: Bcl-2 Protects Macrophages from Nitric Oxide-induced Apoptosis. *J Biol Chem* 1996; 271: 20192–7.
73. <http://www.ncbi.nlm.nih.gov/gene/6352>, retrieved 13. 3. 2013.
74. Sørensen TL, Tani M, Jensen J, Pierce V, Lucchinetti C, Folcik VA, Qin S, Rottman J, Sellebjerg F, Strieter RM, Frederiksen JL, Ransohoff RM: Expression of specific chemokines and chemokine receptors in the central nervous system of multiple sclerosis patients. *J Clin Invest* 1999; 103: 807–15.
75. Palma JP, Kim BS: Induction of selected chemokines in glial cells infected with Theiler's virus. *J Neuroimmunol* 2001; 117: 166–70.

76. Elenkov IJ, Wilder RL, Chrousos GP, Vizi ES: The sympathetic nerve--an integrative interface between two supersystems: the brain and the immune system. *Pharmacol Rev* 2000; 52: 595–638.
77. Laureys G, Clinckers R, Gerlo S, Spooren A, Wilczak N, Kooijman R, Smolders I, Michotte Y, De Keyser J: Astrocytic  $\beta$ 2-adrenergic receptors: From physiology to pathology. *Prog Neurobiol* 2010; 91: 189–99.
78. <http://www.millipore.com/pathways/pathviewer.do?pathwayId=38>, retrieved 14. 3. 2013.
79. <http://www.ncbi.nlm.nih.gov/gene/23657>, retrieved 14. 3. 2013.
80. Pampliega O, Domercq M, Soria FN, Villoslada P, Rodríguez-Antigüedad A, Matute C: Increased expression of cystine/glutamate antiporter in multiple sclerosis. *J Neuroinflammation* 2011; 8: 63.